catalysts

MDPI

Review

Recent Advances on Copper Complexes as Visible Light Photoinitiators and (Photo) Redox Initiators of Polymerization

Guillaume Noirbent * and Frédéric Dumur *

Aix Marseille Univ, CNRS, ICR UMR 7273, F-13397 Marseille, France

* Correspondence: guillaume.noirbent@univ-amu.fr (G.N.); frederic.dumur@univ-amu.fr (F.D.)

Received: 27 July 2020; Accepted: 19 August 2020; Published: 20 August 2020

Abstract: Metal complexes are used in numerous chemical and photochemical processes in organic chemistry. Metal complexes have not been excluded from the interest of polymerists to convert liquid resins into solid materials. If iridium complexes have demonstrated their remarkable photochemical reactivity in polymerization, their high costs and their attested toxicities have rapidly discarded these complexes for further developments. Conversely, copper complexes are a blooming field of research in (photo) polymerization due to their low cost, easy syntheses, long-living excited state lifetimes, and their remarkable chemical and photochemical stabilities. Copper complexes can also be synthesized in solution and by mechanochemistry, paving the way towards the synthesis of photoinitiators by Green synthetic approaches. In this review, an overview of the different copper complexes reported to date is presented. Copper complexes are versatile candidates for polymerization, as these complexes are now widely used not only in photopolymerization, but also in redox and photoassisted redox polymerization processes.

Keywords: copper complex; photoinitiator; photopolymerization; photosensitizer; photoredox catalysis; TADF; redox polymerization; free radical polymerization; cationic polymerization

1. Introduction

Photopolymerization is an old polymerization technique that makes use of light to initiate a polymerization reaction and convert a liquid monomer into a solid material. Photopolymerization offers many attractive features compared to the traditional thermal polymerization such as a temporal and a spatial control so that the polymerization process occurs only during the time for which the light is switched on and within the irradiated zone [1–3]. With regards to the release of volatile organic compounds (VOCs), the polymerization process can be carried out in solvent-free conditions, addressing both the emission of volatiles but also waste treatment issues [4–6]. Therefore, photopolymerization can be considered as a zero-VOC technology. Additionally, no work-up subsequent to the polymerization process is required so that the polymer pieces obtained by photopolymerization are ready to use. This unique ability to provide polymeric materials that can be immediately used after polymerization is nowadays valuated in the emerging 3D and 4D printing technologies [7–10]. In contrast with the traditional thermal polymerization, which require hours to form polymers, by photopolymerization, not only high polymerization rates, but also high final monomer conversions can be obtained within a few minutes. By use of this traceless reagent, which is light, photopolymerization can also be considered as a Green approach to prepare polymers. However, at present, photopolymerization suffers from a major drawback in industry i.e., the use of UV light which is at the origin of safety concerns but also requires expensive and energy-consuming setups to be used [11–13]. Recently, a breakthrough has been achieved with the development of compact, lightweight, and cheap light

sources, namely, the light-emitting diodes (LEDs), whose emission spectra can be perfectly controlled from the UV to the infrared region [14–17]. Considering that UV photopolymerization is more and more contested due to the dangers posed by UV radiations [17–19], alternatives have been actively researched, paving the way towards the development of safer polymerization processes done under visible light and low-light intensity [20]. Beyond the simple safety brought by the use of visible light, another major concern of photopolymerization is the light penetration inside the photocurable resin. Indeed, as shown in Figure 1 for a polystyrene latex with an average diameter of 112 nm containing fillers [21], light penetration can range from 600 µm at 400 nm up to 5 cm at 800 nm, enabling to revolutionize the scope of application of photopolymerization from coatings to the elaboration of thick samples [22]. At present, organic dyes used as visible light photosensitizers of polymerization have been extensively studied [23–26]. Interest for metal-free photoinitiators is notably motivated by the high costs of numerous metal precursors but also by the safety concerns raised by the use of transition metals. Organic dyes and especially push–pull dyes are also characterized by an intense absorption band located in the visible range corresponding to the intramolecular charge transfer band [27–36]. As a result of this, the photoinitiator content can be drastically reduced, addressing the toxicity issue. However, organic dyes are not the only ones capable to exhibit high molar extinction coefficients, and, in the literature, highly efficient photoinitiators of polymerization based on iridium complexes have notably been reported, outperforming benchmark photoinitiators such as phenyl *bis*(2,4,6-trimethylbenzoyl) phosphine oxide (BAPO) or camphorquinone (CQ) [37–42]. Their remarkable efficiencies were notably related to their long-living excited states, enabling the photosensitizers to react efficiently with the different additives introduced into the photocurable resins. If the cost of $IrCl_3.xH_2O$ is approximately 80 €/gram, several attempts were made to develop metal complexes with cheaper metal precursors and complexes based on Zn (II) complexes or Fe (II)/Fe (III) complexes were notably proposed. In this last two cases, metal precursors are really cheaper since the cost for zinc acetate dihydrate ($Zn(OAc)_2$) is reduced to 0.09 €/gram and 3.50 €/gram for iron (II) acetate ($Fe(OAc)_2$).

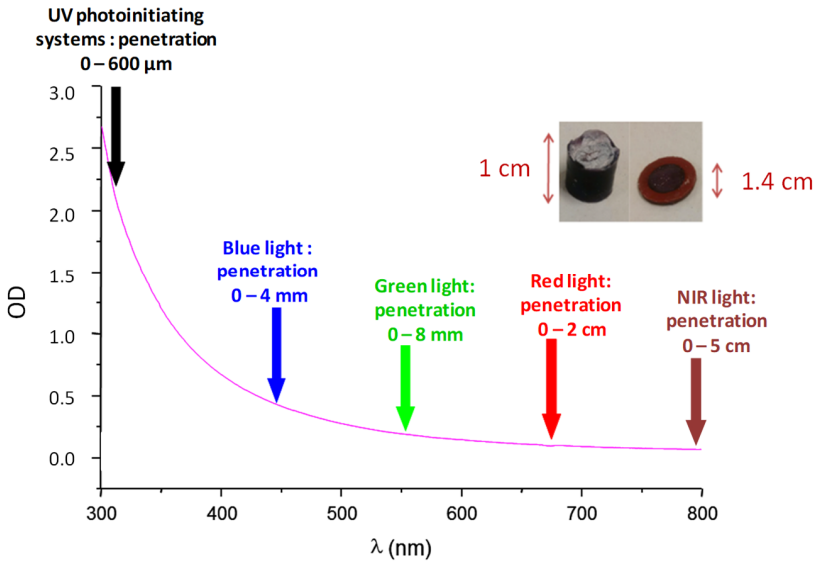

Figure 1. Light penetration inside a polystyrene latex with an average diameter of 112 nm. Inset: examples of polymerized resins containing fillers. Reproduced with permission from the authors of [21]. Copyright 2018 American Chemical Society.

If the Zn precursor is approximately 900 times cheaper than the Ir one, the relatively short-lived excited state of Zn (II) complexes (in the nanosecond scale) made these complexes poor candidates for photoinitiation and only few complexes have been reported as photoinitiators [43–45]. The same holds true for iron complexes bearing Schiff Base ligands [46–50]. Parallel to their short-lived excited state lifetimes, the low photochemical stability of the Schiff Base ligands, their averred instability

under acidic conditions also made this second family of complex a series of metal complexes of poor interest for photoinitiation [51]. However, recently, stability of iron complexes was addressed with the development of ferrocene derivatives, this metallocene being well-known for its remarkable thermal, chemical, electrochemical, and photochemical stability [52,53]. Among metals that could be used to design relatively cheap complexes with long-living excited states, copper can be cited as a relevant example [54–61]. In this field, the pioneering works in photopolymerization have been developed six years ago, in 2014, by the group of Lalevée et al. [62]. However, copper is not an unknown metal in the polymerization field as numerous copper complexes have been developed for thermal atom transfer radical polymerizations (ATRP) [63–65]. Prior to these works, the use of *bis*(amino)acid copper (II) complexes to initiate the polymerization of acrylamide, the use of Cu (I) or Cu (II) salts to photopolymerize tetrahydrofuran, or the use of borate salts to polymerize acrylates can be cited as works reported decades ago [66]. Very recently, in 2018, copper complexes have been involved in a new polymerization approach named metal acetylacetonate–bidentate ligand interaction (MABLI) enabling the formation of acetylacetonate (acac•) radicals by redox reaction with a phosphine and capable to initiate the free radical polymerization (FRP) of acrylates or to promote the free radical promoted cationic polymerization (FRPCP) of epoxides [67–71]. Contrarily to the aforementioned photosensitive complexes (i.e., Ir, Fe, and Zn) which are typically neutral complexes [72,73], copper complexes are generally positively charged so that a counter-anion has to be used. Presence of this counterion ensuring the electrical neutrality of the salt is not without influence on the photoinitiating ability. Indeed, in this field, the role of the counterion on the photoinitiating ability of ionic photoinitiators was remarkably evidenced with a series of iodonium salts differing by their counterions [74]. By using counterions of bigger sizes, the final monomer conversion could be greatly improved, the nucleophilicity of the anion decreasing with the size. Concerning copper complexes, it has to be noticed that in the literature, numerous copper complexes have been reported as being phosphorescent compounds with regards to their excited state lifetimes in the microsecond scale. However, as demonstrated by the extensive works of Chihaya Adachi on the thermally activated delayed fluorescence (TADF) properties since 2012 [75,76], numerous copper complexes previously reported in the literature as phosphorescent complexes are in fact TADF complexes, so that the literature concerning copper complexes has to be considered carefully, in light of this recent discovery [17]. In fact, due to the small energy splitting between the triplet and the singlet excited states, the singlet excited state can be repopulated from the triplet state at room temperature, enabling the observation of an emission from the singlet excited state (delayed fluorescence) and not from the triplet state as observed in the case of phosphorescent materials.

In this review, an overview of the different copper complexes reported to date in polymerization processes is given. To evidence the remarkable initiating ability of these complexes in photochemical, redox and photoredox processes, comparisons with benchmark photoinitiators are provided.

2. Copper Complexes as Visible Light Photoinitiators of Polymerization

2.1. Copper Complexes as Photoredox Catalysts

As discussed in the introduction section, the first report mentioning the use of photosensitive copper complexes in photopolymerization have been reported in 2014 [62]. In this work, two different bulky phosphorylated ligands were used, namely, *bis*(2-(diphenylphosphino)phenyl) ether (DPEPhos) and 4,5-*bis*(diphenylphosphino)-9,9-dimethylxanthene (XantPhos) for the design of **Cu-1-Cu-3** (See Figure 2).

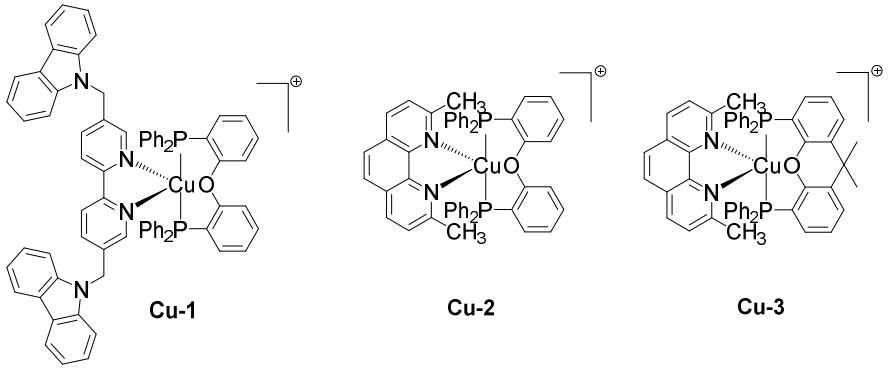

Figure 2. Chemical structures of **Cu-1**–**Cu-3**.

Concerning their syntheses, the three complexes (**Cu-1**–**Cu-3)** could be prepared in high yields using a stepwise approach. By first complexing the bulky phosphorylated ligands (DPEPhos or XantPhos) with one equivalent of tetrakis (acetonitrile)copper (I) tetrafluoroborate ($Cu(CH_3CN)_4.BF_4$) and then opposing the appropriate ancillary ligand to the intermediate complex, a ligand exchange could occur, and the heteroleptic complexes **Cu-1**–**Cu-3** could be prepared with reaction yields ranging from 66% for **Cu-1** to 86% for **Cu-2** (See Scheme 1) [62]. Complexes could also be isolated by precipitation, facilitating the purification process. The way how to recover these complexes is totally different to that used for the previously mentioned iridium complexes that could only be synthesized in low yields, but also required an extensive purification process to be obtained in pure form [37–42].

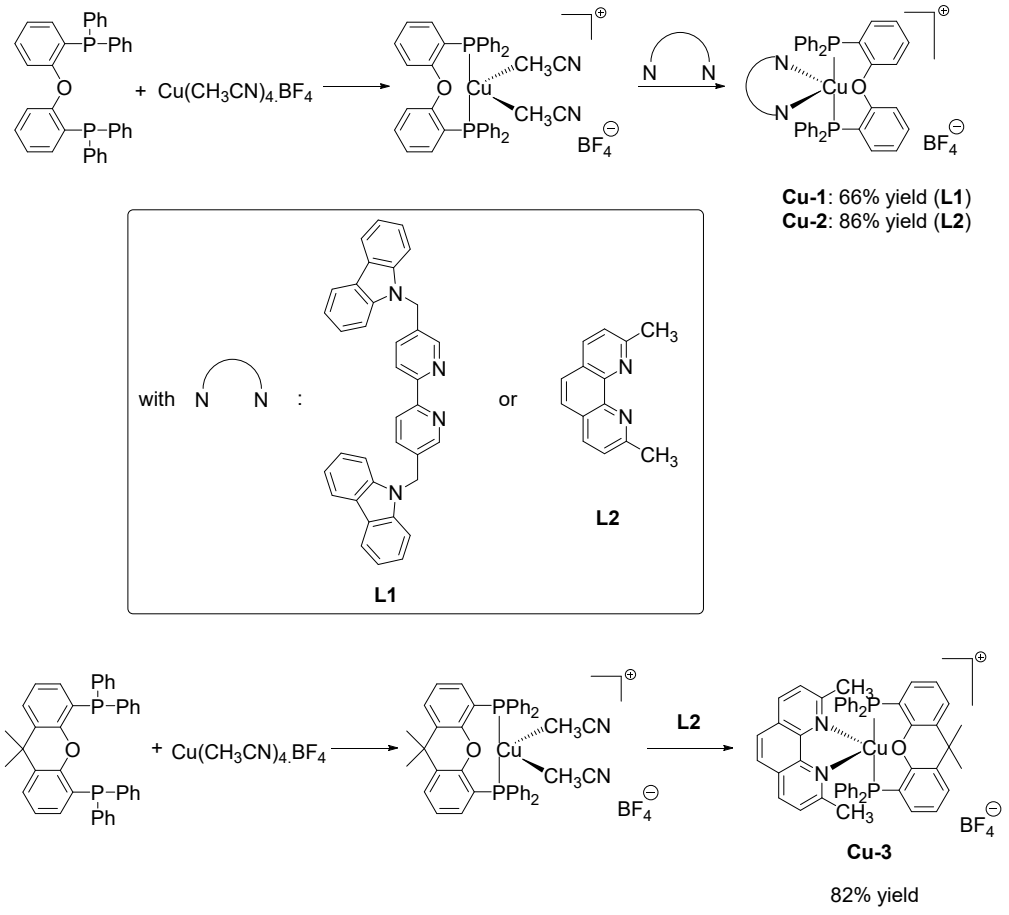

Scheme 1. Synthetic route to **Cu-1**–**Cu3**.

As an interesting feature, the three complexes displayed a strong absorption in the near-visible range, with absorption maxima at 380 nm for **Cu-1** and **Cu-2**, and 383 nm for **Cu-3** (See Figure 3). **Cu-1** showed the broadest absorption of the series, with an absorption extending until 550 nm. Conversely, the absorption of **Cu-2** and **Cu-3** was more restricted, limited to 450 nm. In this context, the photopolymerization tests could be carried out upon excitation with LEDs emitting at 405 nm (110 mW/cm^2) or at 455 nm (80 mW/cm^2), but also with a halogen lamp emitting between 370 and 800 nm (12 mW/cm^2).

Prior to the polymerization tests, examination of the photochemical stability of the different complexes in solution revealed **Cu-2** to be sensitive to the solvent polarity. Thus, irradiation at 405 nm of an acetonitrile solution of **Cu-2** revealed the appearance of a new band in the UV–visible absorption spectrum, assigned to the formation of Cu(**L$_2$**).BF$_4$, consistent with the results previously reported in the literature [77,78]. Indeed, ligand displacement is sometimes observed for sterically hindered complexes upon photoexcitation, during the structural rearrangement from the initial octahedral geometry to the square planar geometry. Conversely, in dichloromethane, no modification of the absorption spectrum was found for **Cu-2** even after 20 min of irradiation at 405 nm [79]. Examination of the **Cu-x (x = 1–3)**/Iod interaction by ESR spin trapping experiments revealed the formation of Ph• radicals, capable to initiate the FRP of acrylates [62]. Upon addition of NVK into the resin, Ph• radicals generated within the resin can add onto the double bond of NVK and produced Ph-NVK• radicals that can be easily oxidized by the iodonium salt, furnishing Ph-NVK$^+$ cations capable to initiate the FRPCP of epoxides (see Figure 4). Noticeably, use of NVK as an additive also allows an efficient regeneration of the photosensitizer, rendering the photoinitiating system catalytic.

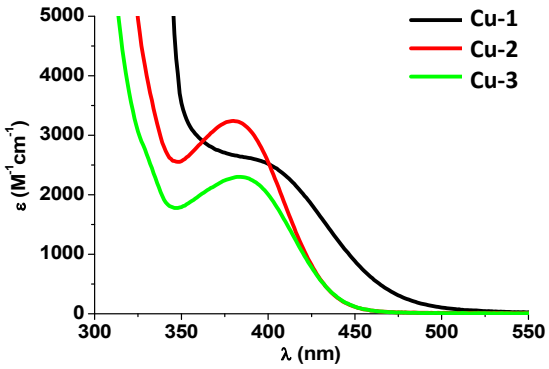

Figure 3. UV–visible absorption spectra of **Cu-1**–**Cu-3** in dichloromethane. Reproduced with permission from the authors of [62]. Copyright 2014 The American Chemical Society.

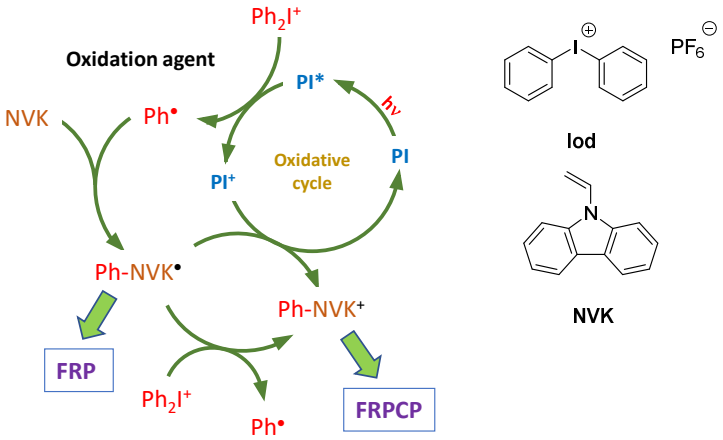

Figure 4. Mechanisms involved in the generation of radicals and cations during the free radical polymerization (FRP) and the free radical promoted cationic polymerization (FRPCP).

The photoinitiating ability of the three complexes was also studied by examining the photolysis of the **Cu-x (x = 1–3)**/Iod system in dichloromethane at 405 nm [62]. Surprisingly, if a very fast photolysis was observed for the **Cu-2**/Iod and **Cu-3**/Iod systems, conversely, a slow bleaching was observed for the **Cu-1**/Iod system. In fact, laser flash photolysis experiments revealed the excited state lifetime of **Cu-1** to be relatively short (<6 ns), what is unfavorable for an efficient interaction between **Cu-1** and Iod and support the poor reactivity of the two-component **Cu-1**/Iod system. On the opposite, excited state lifetimes in the microsecond scale were found for **Cu-2** and **Cu-3**, supporting the fast photolysis in solution. This order of reactivity was confirmed during the free radical polymerization (FRP) of trimethylolpropane triacrylate (TMPTA) (See Figure 5). Thus, a final monomer conversion of 25% and 14% were found, respectively, at 405 nm and 457 nm for the two-component **Cu-1**/Iod (0.2%/2%, *w*/*w*) system after 400 s of irradiation under air, whereas 41% of conversions were determined both at 405 and 457 nm for the two-component **Cu-2**/Iod (0.2%/2%, *w*/*w*) system. Interestingly, the lower monomer conversion obtained with **Cu-3** is directly related to its lower molar extinction coefficient both at 405 and 457 nm compared to that of **Cu-2** (18 and 26% at 405 and 457 nm, respectively) [62]. While adding NVK, the monomer conversion could be increased up to 63% at 405 nm, still upon irradiation for 400 s under air. Comparison with the two-component camphorquinone/*N*-methyldiethanolamine (MDEA) or camphorquinone/Iod systems or the benchmark phenylbis(2,4,6-trimethylbenzoyl) phosphine oxide (BAPO) revealed the three-component **Cu-2**/Iod/NVK (0.2%/2%/3%, *w*/*w*/*w*) system to outperform the three references systems (63% monomer conversion with **Cu-2** vs. 53% for BAPO at 405 nm). While examining the free radical promoted cationic polymerization (FRPCP) of (3,4-epoxycyclohexane) methyl 3,4-epoxy-cyclohexylcarboxylate (EPOX), nor **Cu-1** or **Cu-3** could initiate the FRPCP, irrespective of the photoinitiating systems (two- or three-component systems). Conversely, the photoinitiating ability of the two-component **Cu-2**/Iod (0.2%/2%, *w*/*w*) system remained low, peaking at 13%, upon irradiation at 405 nm for 800 s. Only the three-component **Cu-2**/Iod/NVK (0.2%/2%/3%, *w*/*w*/*w*) system could ensure a reasonable EPOX conversion, reaching 61% in the same conditions under air. The higher reactivity of the three-component system can be assigned to the presence of NVK, generating the highly reactive Ph-NVK$^+$ cation, and the two reaction pathways enabling to form this cation, by reduction of the oxidized form of the copper complex or by reaction of Ph-NVK• with Ph_2I^+ (See Figure 5) [62].

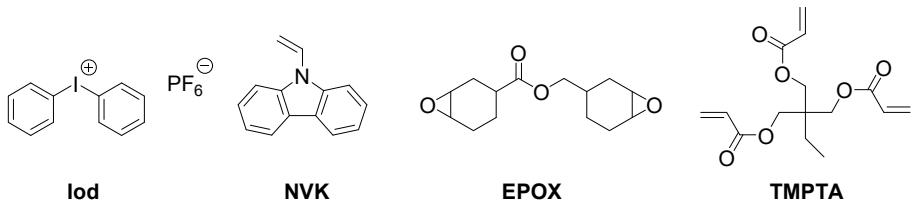

Figure 5. Monomers and additives used with **Cu-1**–**Cu3**.

Finally, by the simultaneous presence of Ph-NVK• and Ph-NVK$^+$ within the resin, the formation of interpenetrated polymer networks (IPNs) resulting from the concomitant polymerization of EPOX and TMPTA could be prepared. Interestingly, two different situations could be evidenced, with a higher monomer conversion of EPOX under air compared to that of TMPTA and the opposite situation in laminate (See Figure 6). These results were assigned to the fact that the FRP of TMPTA was going faster than the FRPCP of EPOX, but also to the fact that under air, part of the generated radicals are consumed by oxygen, reducing the TMPTA conversion.

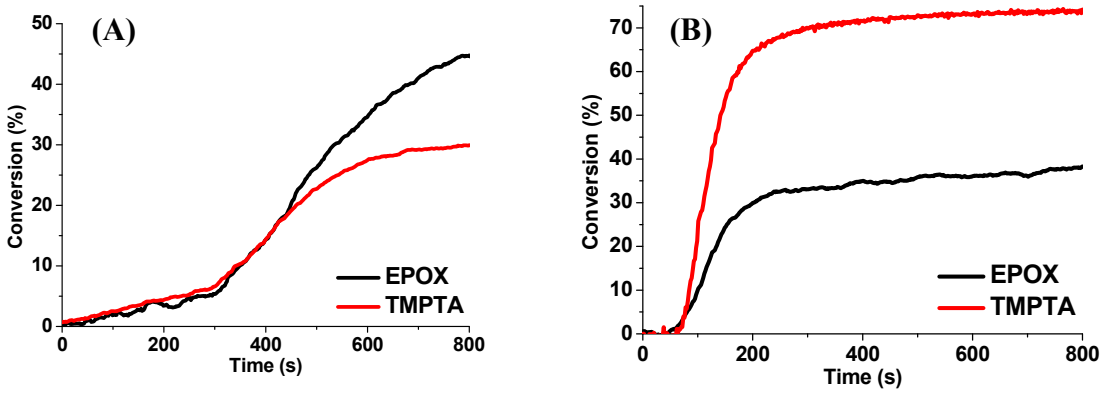

Figure 6. Polymerization profiles of an EPOX/TMPTA blend (50%/50%, *w*/*w*) using the three-component **Cu-2**/Iod/NVK (0.1%/3%/5%, *w*/*w*/*w*) system under air (**A**) and in laminate (**B**), irradiation with a halogen lamp. Reproduced with permission from the authors of [62]. Copyright 2014 The American Chemical Society.

Following these works, the same authors examined the ligand effects with a series of 23 different Cu (I) complexes [80]. As observed for **Cu-1**–**Cu-3**, copper complexes could be clearly divided into two distinct families with regards to their photoinitiating abilities. Thus, the first group of copper complexes contains those bearing ancillary ligands with bulky groups at the inner position of the bipyridine or the phenanthroline ligands such as **Cu-4**–**Cu-9** (see Figure 7). However, among this series, different behaviors were observed. Thus, if **Cu-8** and **Cu-9** proved to be unstable in solution upon irradiation, **Cu-7** was ineffective as photoinitiators of polymerization, irrespective of the conditions used. When tested as photoinitiators in two-component **Cu-x (x = 4–9)**/Iod (0.2%/2% *w*/*w*) systems, final monomer conversions ranging from 20 to 32% at 405 nm, 25 to 49% at 457 nm, and 22 to 46% with a halogen lamp could be determined with the different systems. Comparison with the reference two-component camphorquinone/Iod (0.2%/2% *w*/*w*) system revealed the aforementioned copper-based systems to outperform this benchmark photoinitiator, the monomer conversion peaking only at 18% upon a halogen lamp irradiation (See Table 1).

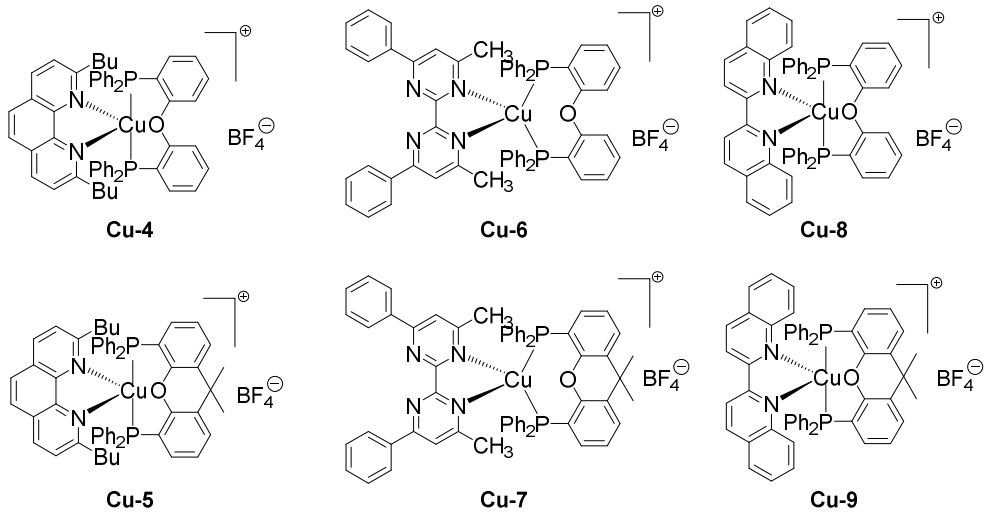

Figure 7. Chemical structures of **Cu-4**–**Cu-9**.

Table 1. TMPTA conversions determined in laminate for two-component systems **Cu-x(x = 4–6)/**Iod (0.2%/2% *w*/*w*) upon irradiation at different wavelengths for 500 s and light absorption properties at the emission wavelengths of the different light sources (extracted from the work in [80]).

	Laser Diode (405 nm)	Laser Diode (457 nm)	Halogen Lamp	ε_{405nm} ($M^{-1}cm^{-1}$)	ε_{457nm} ($M^{-1}cm^{-1}$)
Cu-4/Iod	20%	25%	43%	1500	440
Cu-5/Iod	37%	49%	46%	3100	1000
Cu-6/Iod	32%	36%	22%	4000	1200
CQ/Iod			18% *		

* 400 s of irradiation.

Parallel to this first group, a second group of copper complexes for which no substituent was introduced in *ortho*-position of the pyridinic groups of the ancillary ligands could be identified, comprising **Cu-10**–**Cu20** (See Figure 8). Here, again, several complexes proved to be ineffective candidates for photoinitiation, as exemplified by **Cu-15** and **Cu-16** that are unstable upon irradiation in solution. Conversely, **Cu-17** could not be used as photoinitiator, no photolysis being observed for the **Cu-17**/Iod combination. Stability of the **Cu-17**/Iod combination was assigned to a back electron transfer occurring between Iod and **Cu-17**. For all the other complexes and as shown in the Table 2, an improved photoinitiating ability could be evidenced at 405 nm during the FRP of TMPTA in laminate (21–36% monomer conversion) [80]. Increase of the monomer conversions is directly related to their higher molar coefficients at 405 nm compared to that of the previous series. Conversely, at 457 nm and due to a reduction of the absorption properties of all complexes, lower final monomer conversions could be determined. In this second series of complex, **Cu-18** proved to be the best candidate, even if its light absorption properties were aside from that of **Cu-19** and **Cu-20**. Superiority of **Cu-18** can be confidently attributed to its higher reactivity of **Cu-18** towards the iodonium salt that was clearly demonstrated during the photolysis experiments in solution (faster discoloration of the solution for **Cu-18** vs. **Cu-19** or **Cu-20**). Comparison with **Cu-2** and **Cu-3** previously reported revealed **Cu-18**–**Cu-20** to outperform these two complexes.

Table 2. TMPTA conversions determined in laminate for two-component systems **Cu-x(x = 11–20)/**Iod (0.2%/2% *w*/*w*) and three-component systems **Cu-x(x = 2,3,18)/**Iod/NVK (0.2%/2%/3% *w*/*w*/*w*) upon irradiation at different wavelengths for 500 s and light absorption properties at the emission wavelength of the light sources (extracted from the work in [80]).

	Laser Diode (405 nm)	Laser Diode (457 nm)	Halogen Lamp	ε_{405nm} ($M^{-1}cm^{-1}$)	ε_{457nm} ($M^{-1}cm^{-1}$)
Cu-10/Iod	30%	42%	25%	3100	400
Cu-11/Iod	21%	38%	21%	2500	350
Cu-12/Iod	32%	<5%	19%	2600	150
Cu-13/Iod	36%	18%	8%	2000	120
Cu-14/Iod	33%	15%	16%	2500	180
Cu-18/Iod	36%	51%	50%	5500	1200
Cu-19/Iod	34%	52%	49%	4800	2000
Cu-20/Iod	30%	48%	46%	6300	2600
Cu-18/Iod/NVK		59%	57%		
Cu-2/Iod	41%	41%	48%		
Cu-2/Iod/NVK			56%		
Cu-3/Iod	21%	38%	38%		
Cu-3/Iod/NVK		41%	42%		

Finally, the high monomer conversion achieved with the three-component **Cu-18**/Iod/NVK (0.2%/2%/3% *w*/*w*/*w*) upon introduction of NVK in the photocurable resin can be assigned to the

regeneration of the photosensitizer in this case, rendering the photoinitiating system catalytic (See Figure 4) [80].

Here again, superiority of **Cu-18** over **Cu-2** and **Cu-3** was demonstrated in the three-component system **Cu-x**/Iod/NVK (0.2%/2%/3% *w*/*w*/*w*), an enhancement of the monomer conversion by ca. 20% being compared to that of **Cu-3**. As interesting feature, **Cu-18** proved not only to be an efficient photoinitiator in an oxidative mechanism but also a reductive one when opposed to an amine (methyl diethanolamine (MDEA). Upon excitation by light, a photoinduced electron transfer between **Cu-18** and MDEA occurs, producing radicals by hydrogen abstraction. In the presence of an oxidation agent, **Cu-18** can be reoxidized by the oxidizing agent (R-Br), providing a second source of radicals (See Figure 9). In this context of dual source of radicals, final monomer conversions comparable to that obtained with the oxidative mechanism could be determined with **Cu-18** as the sensitizer (See Table 3). Here, again, **Cu-18** proved to be a better photoinitiator than benchmark photoinitiators such as BAPO or camphorquinone [80].

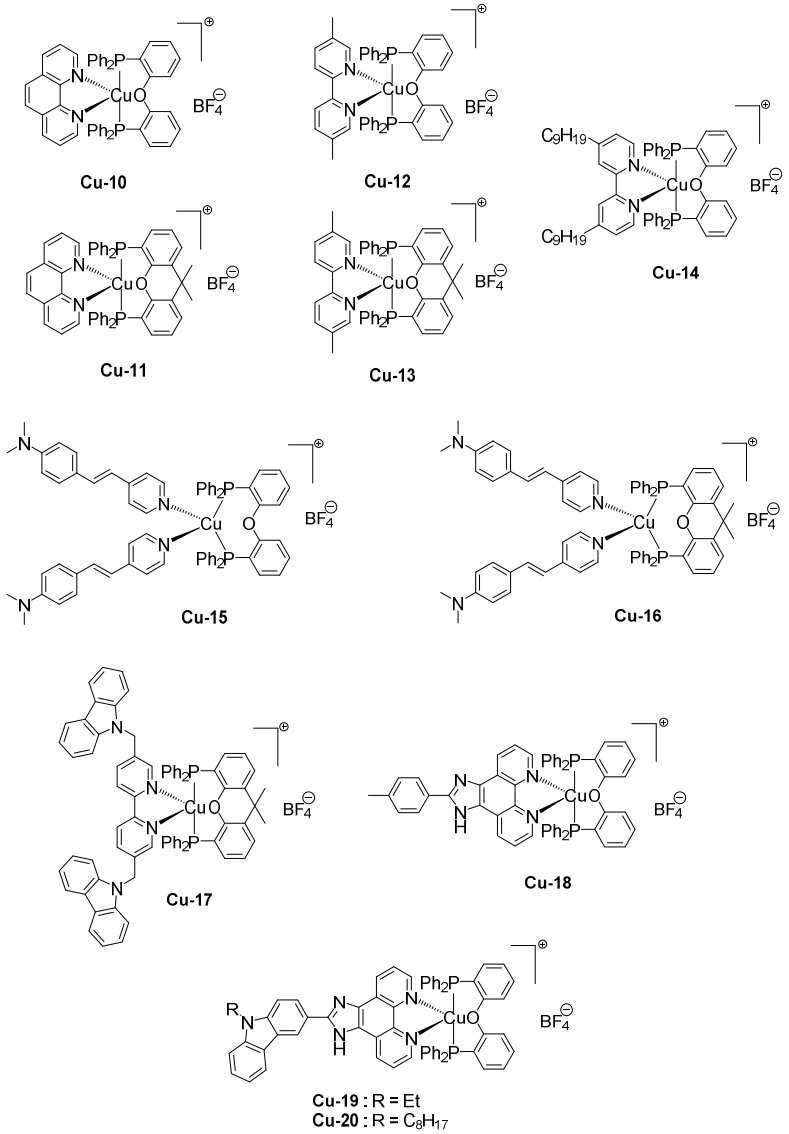

Figure 8. Chemical structures of **Cu-10**–**Cu-20**.

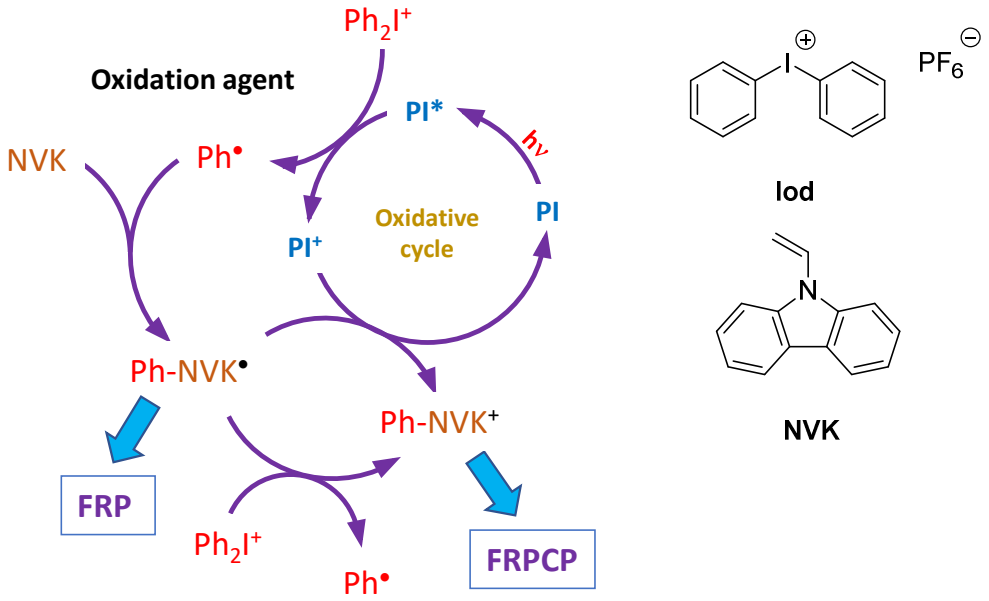

Figure 9. Chemical mechanism involved in the generation of radicals in the reductive cycle.

Table 3. TMPTA conversions determined in laminate upon irradiation at different wavelengths of the three-component system **Cu-18**/R-Br/MDEA (0.2%/2%/3% *w*/*w*/*w*) for 500 s and light absorption properties at the emission wavelength of the light sources (extracted from the work in [80]).

	LED (405 nm)	LED (455 nm)	Halogen Lamp	$\varepsilon_{405\ nm}$ ($M^{-1}cm^{-1}$)	$\varepsilon_{457\ nm}$ ($M^{-1}cm^{-1}$)
Cu-18/R-Br/MDEA	59% *	55% *	49% *	5500	1200
BAPO	53% *				
CQ/MDEA			35% *		

* 400 s of irradiation.

Finally, an examination of homoleptic complexes such as **Cu-21**–**Cu-26** as photoinitiators revealed their poor ability in the visible range, with only **Cu-25** being capable to initiate the FRP of TMPTA at 457 nm (38% conversion with the three-component **Cu-25**/Iod/NVK (0.2%/2%/3% *w*/*w*/*w*) system (see Figure 10). For the other complexes, their lack of absorption in the visible range makes these complexes unsuitable candidates for visible light photopolymerization. It has to be noticed that if no efficient TMPTA polymerization could be achieved with **Cu-24** in this work, recent works have nonetheless demonstrated the possibility to photocatalyze an atom transfer radical polymerization under visible light, upon irradiation at 405 nm [81].

Returning to **Cu-18**, the same authors also demonstrated the possibility for this complex to act as a photoredox catalyst for the thiol-ene polymerization of a *tris*(3-mercaptopropionate) (trithiol)-triethyleneglycol divinyl ether (DVE-3) blend (57%/43%, *w*/*w*) (see Figure 11). Upon irradiation with a laser diode at 457 nm, final monomer conversions of 57 and 85% could be, respectively, determined for trithiol and DVE-3, following the mechanism depicted in Equations (1)–(3) [80].

$$Ar\bullet + RSH \rightarrow ArH + RS\bullet \quad (1)$$

$$RS\bullet + DVE\text{-}3 \rightarrow RS\text{-}DVE\text{-}3\bullet \quad (2)$$

$$RS\text{-}DVE\text{-}3\bullet + RSH \rightarrow RS\text{-}DVE\text{-}3\text{-}H + RS\bullet \quad (3)$$

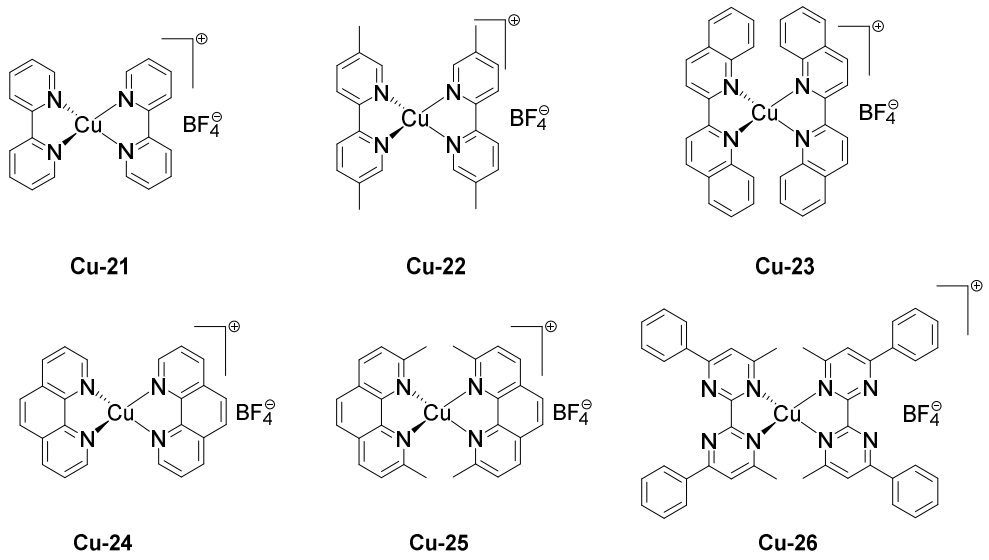

Figure 10. Chemical structures of **Cu-21**–**Cu-26**.

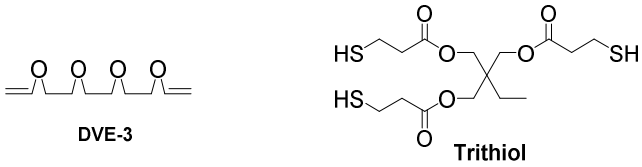

Figure 11. Chemical structures of monomers used for the thiol-ene reaction with **Cu-18**.

In 2017, a series of homoleptic and heteroleptic complexes **Cu-27**–**Cu-33** based on pyridine-pyrazole ligands was evaluated as photoredox catalysts for the FRP of acrylates and the FRPCP of epoxides (see Figure 12) [82]. As interesting features, the charge transfer occurring from the copper center to the diimine ligand in the excited state was highly dependent of the substitution pattern of the diimine ligand, which was confirmed by examining the absorption spectra of **Cu-27**–**Cu-31** [83,84]. Thus, introduction of an electron-withdrawing group onto the ancillary ligand red-shifted the absorption towards the visible range so that the nitro-substituted complex **Cu-31** showed the most red-shifted absorption of the series (λ_{max} = 450 nm). Examining the free energy change ΔG_{et} for the electron transfer reaction between the Cu(I) complexes and Iod determined by using the classical Rehm–Weller equation revealed the electron transfer to be highly favorable for **Cu-27**–**Cu-31** [85]. Conversely, the same values determined for **Cu-32** and **Cu-33** made these two complexes unfavorable candidates for photoinitiation. Final monomer conversions determined for the cationic polymerization of EPOX with the two-component **Cu-x**/Iod (0.5%/1% *w*/*w*) systems followed the order of their absorption abilities at 405 nm and decreased from 48% for **Cu-30** to 45% for **Cu-29**, 18% for **Cu-28**, and 6% for **Cu-27** for an irradiation done at 405 nm during 800 s [82]. Interestingly, no polymerization could be initiated with **Cu-31** in these conditions, **Cu-31** nevertheless exhibiting the most red-shifted absorption of the series and being the complex the most adapted for an irradiation at 405 nm. By adding 9*H*-carbazole-9-ethanol (CARET) as an additive, a behavior similar to that observed with NVK was observed, significantly improving the monomer conversion [86]. Thus, a final monomer conversion of 63% was obtained after 800 s of irradiation at 405 nm with the three-component **Cu-30**/Iod/CARET (0.5%/1%/1% *w*/*w*) system, increased by ~15% compared that obtained with the two-component **Cu-30**/Iod (0.5%/1% *w*/*w*) system. This enhancement can be assigned to the efficient regeneration of **Cu-30** by CARET, avoiding the consumption of the photosensitizer during the polymerization process. Noticeably, a similar enhancement could be obtained with the two-component **Cu-x**/Iod (0.5%/1% *w*/*w*) systems by modifying the counter-anion. Thus, exchange of the BF_4^- anion for the less nucleophilic PF_6^- anion enabled to get comparable enhancements, the monomer conversion

for EPOX increasing from 45% to 63% with **Cu-29**. This trend is consistent with that observed in previous works reported in the literature [87–89]. The order of reactivity determined for the CP of EPOX was confirmed during the FRP of acrylates (TMPTA) or during the FRP of methacrylates while using a dental resin consisting in a bisphenol A-glycidyl methacrylate (BisGMA)/triethyleneglycol dimethacrylate (TEGDMA) (70%/30% *w*/*w*) blend [90–92]. Remarkably, colorless coatings could be obtained with **Cu-30**, as shown in Figure 13.

Considering the high reactivity of the three-component system **Cu-30**/Iod/ethyl 4-(dimethylamino) benzoate (EDB) (0.5%/1%/1% *w*/*w*/*w*) for the photopolymerization of the methacrylate (BisGMA/TEGDMA) resin, surface patterning experiments could be carried out and letters, numbers or figures could be produced with a high precision using a 1951 US Air Force (USAF) resolution calculator (See Figure 14).

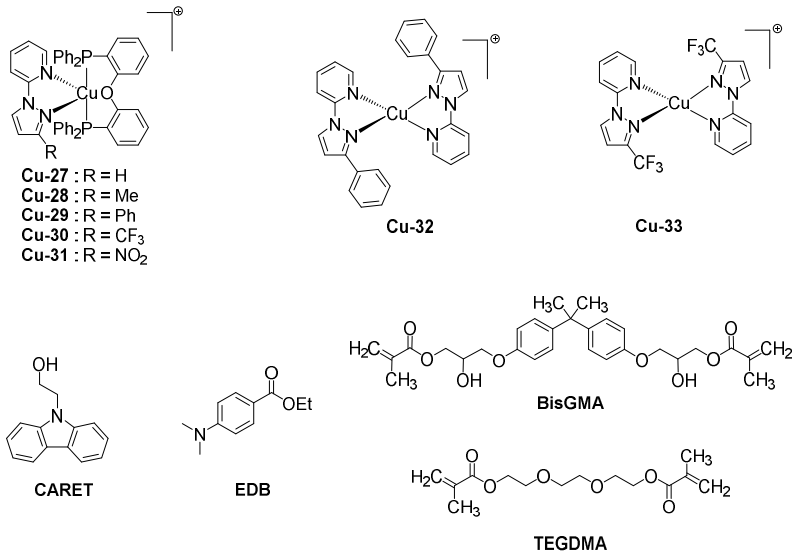

Figure 12. Chemical structures of **Cu-21**–**Cu-26**.

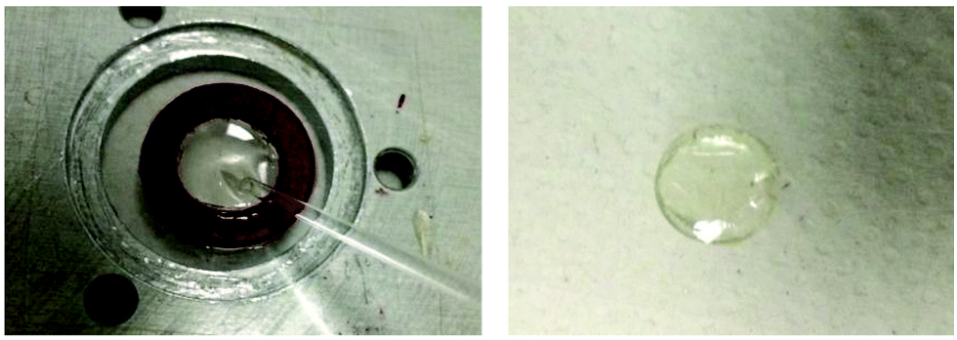

Figure 13. Colorless coatings obtained upon photopolymerization of a BisGMA/TEGDMA (70%/30% *w*/*w*) blend at 405 nm with the two-component **Cu-30**/Iod (0.5%/1% *w*/*w*) system upon photopolymerization of a thick sample (1.4 mm) under air. Reproduced with permission from the authors of [82]. Copyright 2017 The Royal Society of Chemistry.

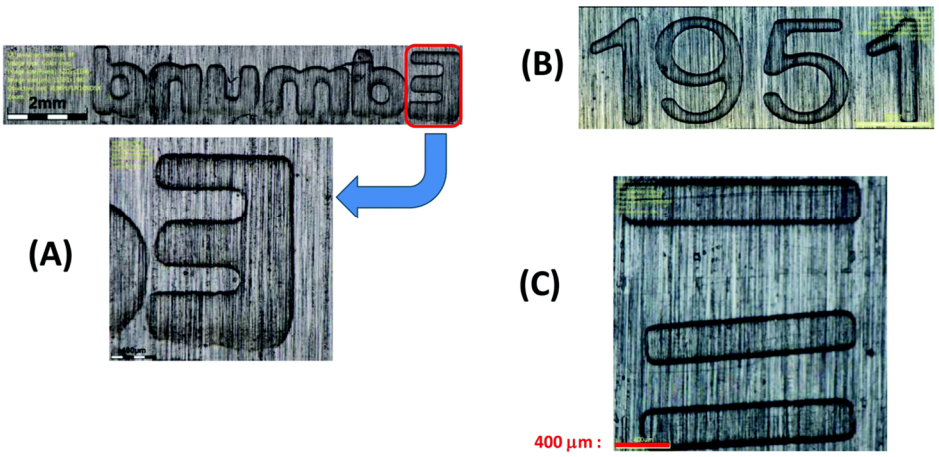

Figure 14. Examples of surface patterning realizing with a LED projector at 405 nm and imaged with a numerical optical microscope using a 1951 USAF resolution test target. (**A**) different letters written (**B**) 1951 (**C**) straight lines. Reproduced with permission from the authors of [82]. Copyright 2017 The Royal Society of Chemistry.

In 2019, **Cu-32** was revisited in the context of the development of antibacterial coatings [93]. A remarkable antibacterial activity against two bacteria i.e., *Escherichia coli* (*E. coli*) and *Staphylococcus aureus* (*S. aureus*) was demonstrated, with a reduction of the proliferation by approximately 99.9 and 96% for the two bacteria, respectively. Especially, the antibacterial activity of the polymer films was determined as originating from the release of Cu^{2+} cations within the polymer films.

2.2. Copper Complexes as Photoinitiators for Polymerization Processes in Shadowed Area

Photopolymerization is a technique widely used to initiate free radical polymerization reactions and exposure of the surface to light is required to generate the reactive species. Besides, photopolymerization is not limited to the polymerization of coatings on planar surfaces and objects with complex structures requiring their surfaces to be coated with a polymer film are more representative of the real applications of photopolymerization in industry. In this context, the development of photocurable resins in which radicals can diffuse until regions that will not be exposed to light is an important challenge. By contrast to the traditional formulations for which a perfect spatial control is required, notably for 3D-printing applications, a totally different approach should be used in the context of polymerization in shadowed area. This phenomenon is named dark polymerization. Among the different approaches reported in the literature, one of the most convenient ways to initiate a dark polymerization consists in generating latent species that will react in the zones not exposed to light. To illustrate this, photoinitiation of a polymerization process with the three-component rose Bengal/ferrocenium salt/amine system comprising a fourth component, i.e., an initiating species (hydroperoxide), constitutes a first approach for the polymerization of thick pigmented films [94,95]. More recently, an elegant strategy was developed with the methylene blue/amine combination with which light irradiation formed a metastable leuco form of methylene blue that could react with an iodonium salt and generate initiating radicals Ar• [96]. A propagation of the polymerization until 3.5 mm from the irradiated zone could be obtained. However, one drawback of this approach was the toxicity of the dye [97–99]. In 2017, an unprecedented strategy was proposed with **Cu-4** [28]. Considering that in the previous photopolymerization experiments done under air with **Cu-4**, an induction period corresponding to the consumption of oxygen by the initiating R′• radicals was typically observed on the polymerization profiles while using the two-component **Cu-4**/Iod system (see Equation (4)), an original strategy consisted in taking advantage of the dissolved oxygen in resins to generate latent species. Indeed, peroxyl radicals R′OO• formed by reaction of R′•

with oxygen can constitute latent species for polymerization processes in shadowed areas by hydrogen abstraction, following the mechanism proposed in Equation (5).

$$R'^{\bullet} + O_2 \rightarrow R'OO^{\bullet} \quad (4)$$

$$R'OO^{\bullet} + R\text{-}H \rightarrow R'OOH + R^{\bullet} \quad (5)$$

Parallel to the photoinitiated process, redox potentials of **Cu-4** are also adapted to induce redox reactions with peroxides such as R'OOH so that R'O• and R'OO• radicals can be simultaneously generated in situ by redox reactions with **Cu-4** (II) and **Cu-4** (I) (see Equations (6) and (7)).

$$Cu\ (I) + ROOH \rightarrow Cu\ (II) + RO\bullet + OH \quad (6)$$

$$Cu\ (II) + ROOH \rightarrow Cu\ (I) + ROO\bullet + H^{+} \quad (7)$$

To avoid the formation of the less reactive ROO• radicals, introduction of a reductant that could reduce Cu (II) into Cu (I) was introduced, favoring Equation (6) over Equation (7). To optimize the initiating system and mutualize as much as possible the different additives used for both the redox and the photochemical mechanisms, the reductant used for the redox system can also be the same as that used in the photochemical mechanism. This goal was achieved by using Tin (II) 2-ethylhexanoate (Tin (II)) that could be simultaneously used for the photochemical and the redox polymerizations (see Figure 15). To favor the diffusion of radicals within the resin as well as oxygen diffusion, a resin of low viscosity was employed, composed of a mixture of three monomers, namely 1,4-butanediol-dimethacrylate (1,4-BDMA) (33 wt%), hydroxypropyl methacrylate (HPMA) (33 wt%) and urethanedimethacrylate (UDMA) (33 wt%). To evidence the reactivity of these hydroxyl radicals, a comparison with cumene hydroperoxide R"OOH was established [28].

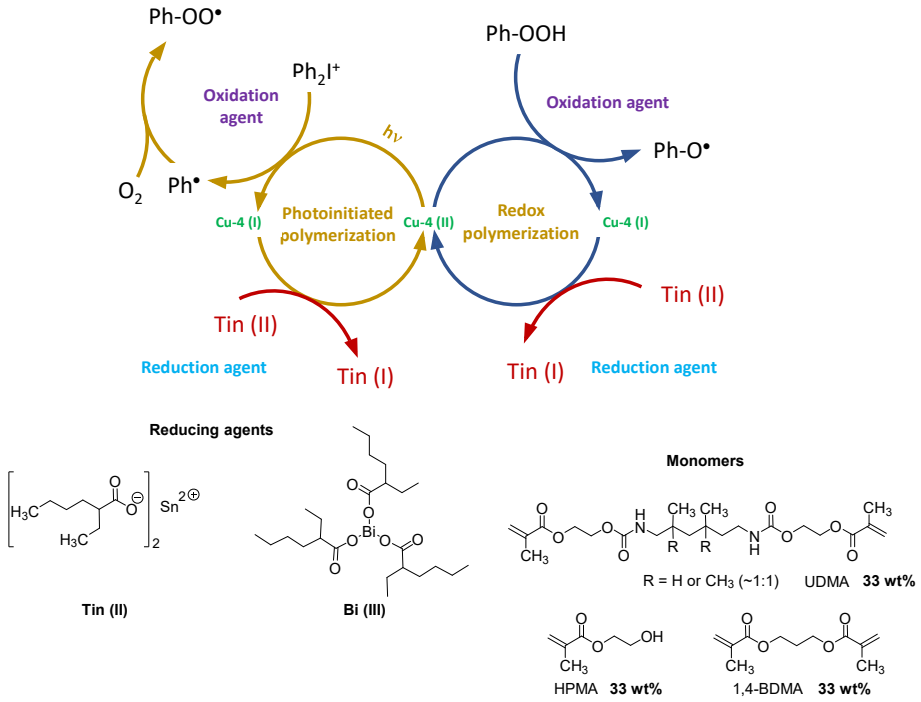

Figure 15. Concomitant photo and redox mechanisms involved in the polymerization in irradiated and shadowed areas. Chemical structures of the reducing agents and monomers used in this study.

As the first finding, the final monomer conversion could be finely tuned by mean of the light intensity. Thus, by maintaining the light irradiation at 35 mW/cm^2, the monomer conversion could be drastically increased by replacing the two-component system **Cu-4**/Iod (0.3%/0.85% *w*/*w*) by the

three-component system **Cu-4**/Iod/Tin (II) (0.3%/0.85%/6% *w*/*w*/*w*). Therefore, an enhancement of the final monomer conversion from 60 to 84% could be obtained within 150 s while regenerating the photosensitizer (see Figure 16) [28].

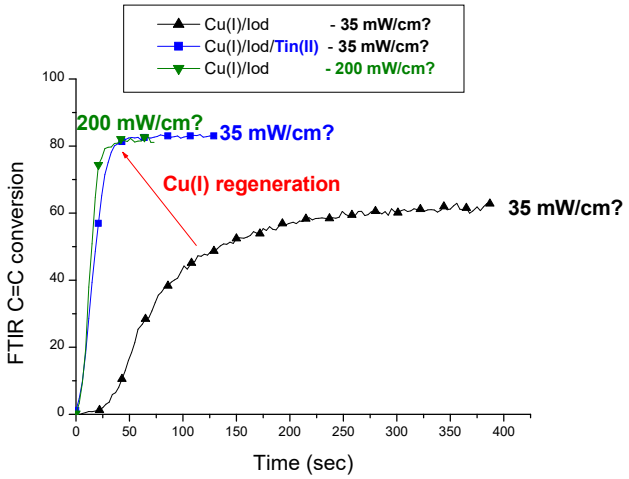

Figure 16. Polymerization profiles of the mixture of monomers by varying the light intensity upon irradiation with a LED@405 nm under air, 1.4 mm thick samples. Reproduced with permission from the authors of [28]. Copyright 2017 American Chemical Society.

Examination of the ability of the three-component system to initiate a polymerization far from the irradiation point was realized by using a Pasteur pipette filled with the resin and by only irradiating the extremity of the Pasteur pipette. Using this strategy, a polymerization extending until 9 cm from the irradiation point could be observed, by breaking the Pasteur pipette and by measuring the length of the resulting polymer (see Figure 17) [28]. To monitor the polymerization process, a thermal imaging camera was utilized. This approach is relatively new in photopolymerization and can be assigned to the recent availability of cheap, easy-to-handle, and precise thermal imaging cameras on the market. As a result of this, thermal imaging can now be used to follow numerous chemical transformations. Indeed, the polymerization of acrylates and methacrylate is known to be exothermic [100,101] so that the polymerization process could be monitored by measuring the variation of temperature during the polymerization reaction.

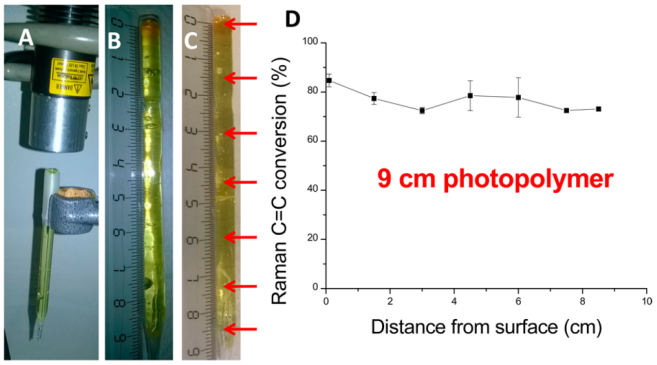

Figure 17. (**A**) Experimental set-up used to examine the polymerization in shadowed areas. (**B**) The Pasteur pipette with the resin before irradiation. (**C**) The resulting polymer obtained after polymerization. (**D**) Final monomer conversion vs. the distance of the irradiation point. Reproduced with permission from the authors of [28]. Copyright 2017 American Chemical Society.

Considering the high reactivity of the three-component system **Cu-4**/Iod/Tin (II) (0.3%/0.85%/6% *w*/*w*/*w*), polymerization of filled samples was examined (See Figure 18). Despites the presence of

fillers, only a minor reduction in the polymer length was found, decreasing from 0.5 cm. Finally, comparison of the ability of the three-component system **Cu-4**/Iod/Tin (II) (0.3%/0.85%/6% *w*/*w*/*w*) with systems previously reported in the literature and examined in the same irradiation conditions revealed the three-component system **Cu-4**/Iod/Tin (II) (0.3%/0.85%/6% *w*/*w*/*w*) to outperform these reported systems (see Figure 19) [28] Thus, if the polymerization reaction could propagate until 3 mm from the irradiated zone with the MB^+/DIPEA/DPI^+ (0.4%/0.2%/0.04% *w*/*w*/*w*) [96], a ten-fold enhancement of the length could be obtained with the three-component system **Cu-4**/Iod/Tin (II) (0.3%/0.85%/8% *w*/*w*/*w*), reaching 32 mm. Concentration of the copper complex was determined as being the key-parameter governing the lateral polymerization, a 6-fold increase of the concentration resulting in a 4-fold enhancement of the polymer length.

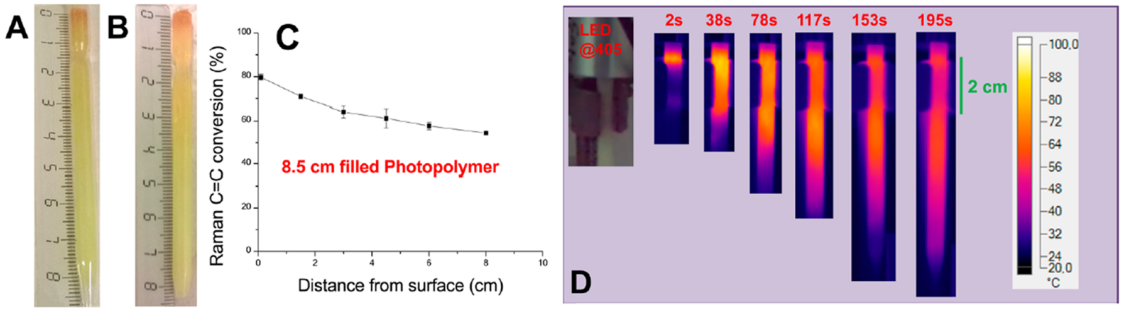

Figure 18. Pasteur pipette containing the resin before (**A**) and after (**B**) breaking the pipette; (**C**) monomer conversion as a function of the distance; (**D**) evolution of the temperature as a function of the reaction time followed by infrared thermal imaging camera. Reproduced with permission from the authors of [28]. Copyright 2017 American Chemical Society.

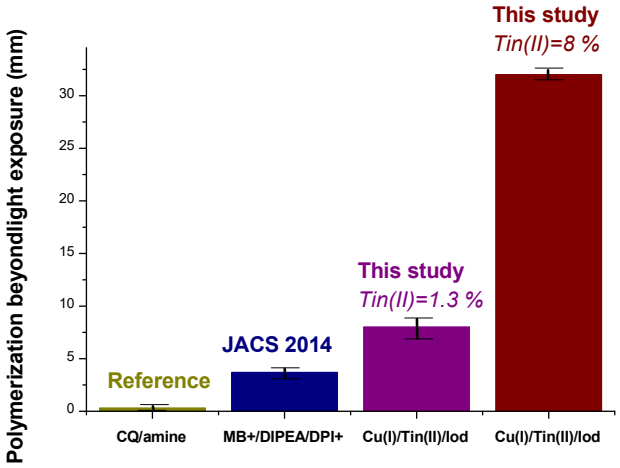

Figure 19. Determination of the polymerization length beyond the irradiated area using different systems previously reported in the literature (camphorquinone/amine: 0.4%/2% *w*/*w* and MB^+/DIPEA/DPI^+: 0.4%/0.2%/0.04% *w*/*w*/*w*) and Cu (I)/Iod/Tin (II) 0.17%/2%/1.3 *w*/*w*/*w* and Cu (I)/Iod/Tin (II) 0.17%/2%/8 *w*/*w*/*w* examined in this study. Reproduced with permission from the authors of [28]. Copyright 2017 American Chemical Society.

Finally, in light of the exceptional reactivity of the three-component system **Cu-4**/Iod/Tin (II) (0.2%/1%/5% *w*/*w*/*w*), the possibility to use sunlight to initiate the polymerization was examined [28]. If the Sun delivers only a limited irradiance (6 mW/cm^2), it constitutes however an interesting light source. Using sunlight, a final monomer conversion of 70% for the methacrylate resin could be obtained within 100 s during a sunny day (see Figure 20). If a reduction of the monomer conversion is observed with sunlight compared to that obtained with a LED at 405 nm (82% monomer conversion, see Figure 17), the decrease remains however limited.

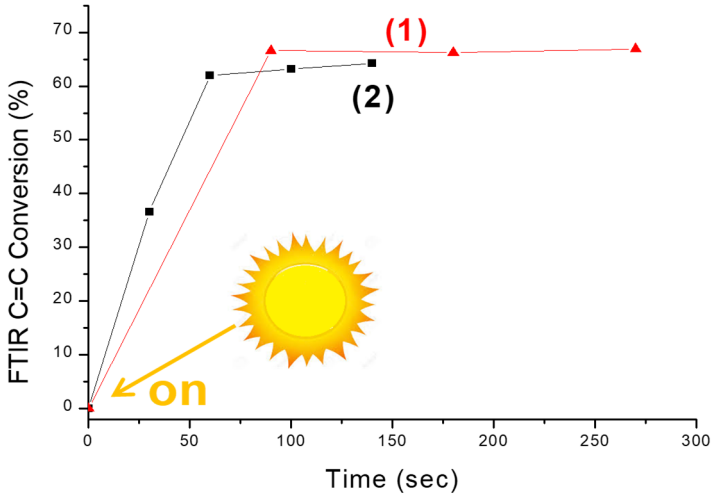

Figure 20. Photopolymerization profiles of the mixture of the methacrylate monomers using the three-component **Cu-4**/Iod/Tin (II) (0.2%/1%/5% *w*/*w*/*w*). Two different experiments were carried out to evidence the reproducibility. With sunshine (**1**) and without sunshine (**2**), reproduced with permission from the authors of [28]. Copyright 2017 American Chemical Society.

2.3. Copper Complexes as Photoinitiators for Dark Polymerization Processes

Cu-4 is a promising photosensitizer for future industrial developments and several studies were devoted to examine its photoinitiating ability with industrial resins (see chemical structures of the model resin in Figure 21) [102,103]. For comparison, BAPO, which is also widely used in industry, was used for comparison.

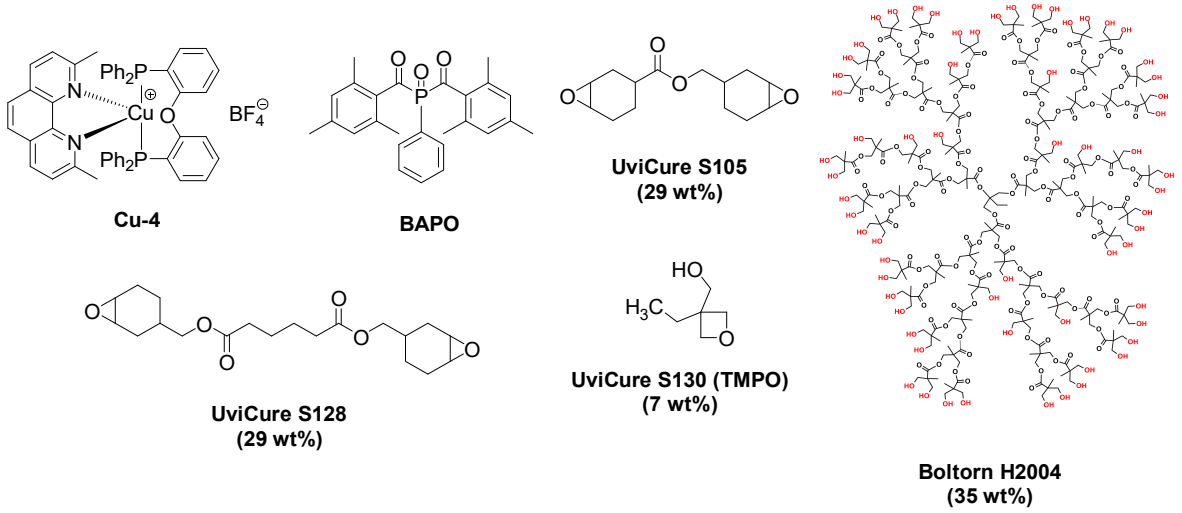

Figure 21. Chemical structures of monomers used in industries.

An interesting finding was the ability of **Cu-4** to give rise to a dark polymerization process, even after irradiation of the photocurable resin during a short time. As shown in the Figure 22, after 60 s of irradiation and by switching the light off, an increase of 22% of the monomer conversion could be monitored by FTIR, whereas the dark polymerization with BAPO was more limited, increase of the monomer conversion being only of 12% [102]. To explain this, the high reactivity of **Cu-4** in three-component systems and thus its ability to generate numerous radicals without a short reaction time but also the higher molar extinction coefficient of **Cu-4** compared to BAPO at 405 nm were suggested as parameters supporting the remarkable dark polymerization observed with **Cu-4**.

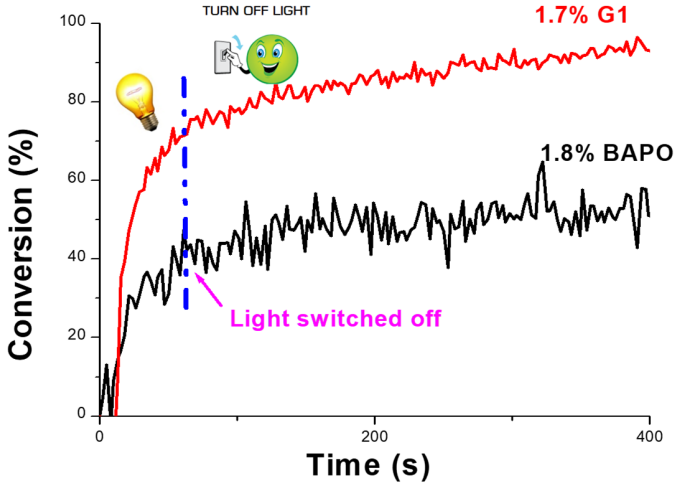

Figure 22. Photopolymerization profiles of the model resin under air with the three-component systems **Cu-4**/Iod/NVK (1.7/4.6/1 *w*/*w*/*w*%) and BAPO/Iod/NVK (1.8/5/1 *w*/*w*/*w*%) upon irradiation with a LED at 405 nm for 400 s. Reproduced with permission from the authors of [102]. Copyright 2017The Royal Society of Chemistry.

2.4. Green Approach towards the Synthesis of Copper-Based Photoinitiators of Polymerization

Synthesis of photoinitiators by Green synthetic routes is an active research field, and, in 2018, the synthesis of **Cu-2** was newly examined in the context of mechanochemistry [104]. Indeed, the synthesis of photoinitiators in solution and the associate waste treatment can constitute a major obstacle for further developments and commercialization of photoinitiators. Mechanosynthesis underwent a revival of interest approximately ten years ago [105–111], by offering a unique opportunity to produce molecules by mean of safer, cleaner, and faster transformations than that proposed by the traditional solution-phase chemistry [112–114]. Mechanochemistry can also give access to molecules that are impossible to reach in solution phase chemistry [115–119] and a relevant example of this was provided **Cu-2** bearing an iodide counteranion. Indeed, due to the low ionicity of the Cu–I bond (~12%), this bond cannot be dissociated in solution. On the opposite, forces brought by mechanochemistry are different from those obtained by heating in solution phase chemistry so that **Cu-2**.I could be obtained in 70–72% yield with a purity higher than 95% (See Scheme 2).

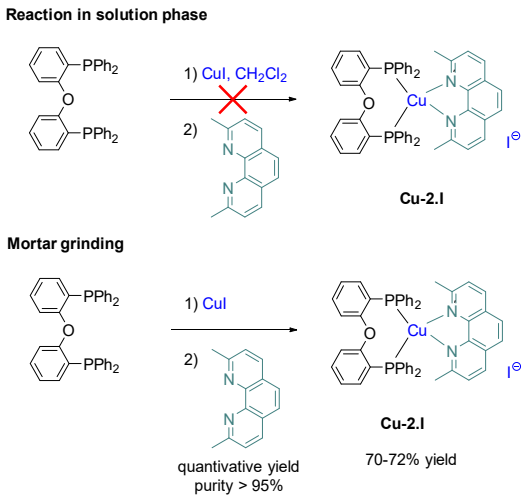

Scheme 2. Chemical route to **Cu-2**.I by mechanochemistry.

However, grinding of the powder for 30 min was necessary to produce the complex. Conversely, reduced reaction times were required to prepare **Cu-2**.PF_6 and **Cu-2**.BF_4 as the two complexes **Cu-2**.PF_6

and **Cu-2**.BF_4 could be prepared in quantitative yields within 5 min with purities comparable to that obtained in solution (See Figure 23). This corresponds to a 170-fold reduction of the reaction time compared to that required in solution (5 min against 14 h) [104].

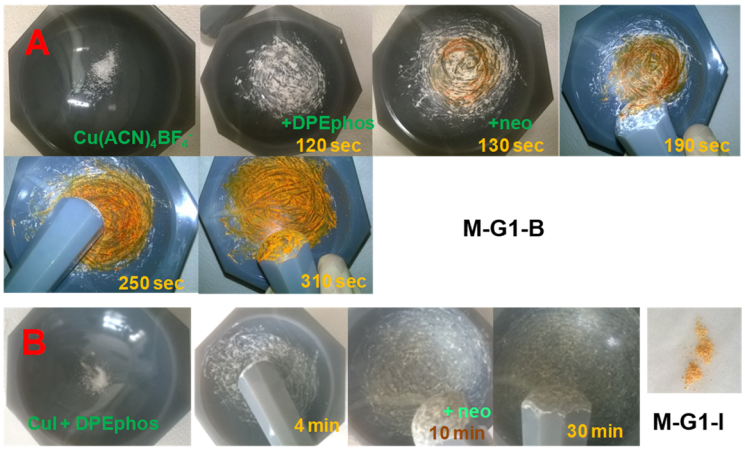

Figure 23. Mechanosynthesis of **Cu-2**.BF_4 (**A**) and **Cu-2**.I (**B**). Reproduced with permission from the authors of [104]. Copyright 2018 American Chemical Society.

While using the two-component **Cu-2.**PF_6/(*tert*-Bu)Ph_2I^+ (0.3%/0.8%, *w*/*w*) system for the polymerization of a methacrylate resin of low viscosity (see chemical structures in Figure 15), comparison of the polymerization profiles obtained for the photosensitizer prepared in solution or by mechanochemistry revealed similar polymerization rates and similar final monomer conversions, evidencing the pertinence of the approach (See Figure 24a) [104]. Here, again, by increasing the light intensity from 35 mW/cm^2 to 110 mw/cm^2, a 20-fold reduction of the reaction time was required to get 60% monomer conversion with the mechanosynthesized **Cu-2.**PF_6 (See Figure 24a,b).

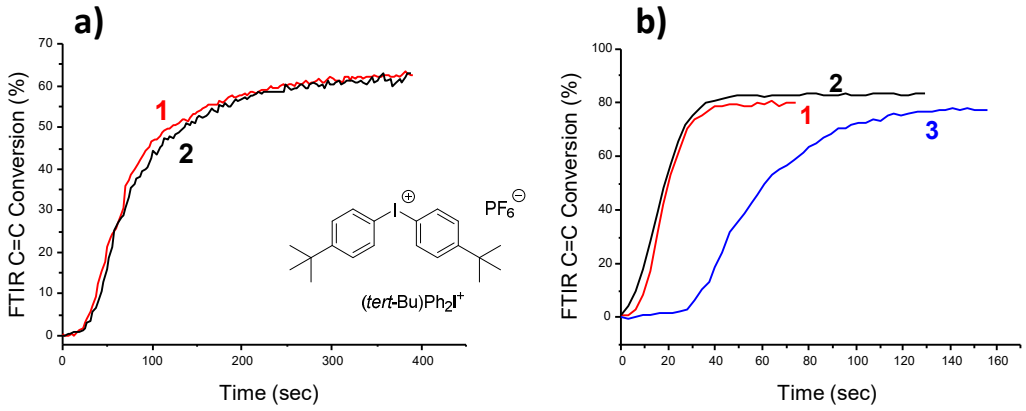

Figure 24. (**a**) Comparison of the polymerization profiles obtained for the FRP of the methacrylates resin using **Cu-2**.PF_6 prepared by mechanochemistry (1) and **Cu-2**.BF_4 in solution (2) in two-component **Cu-2**/(*tert*-Bu)Ph_2I^+ (0.3%/0.8% *w*/*w*) systems upon exposure to a LED at 405 nm (35 mW/cm^2). (**b**) Comparison of the polymerization profiles obtained with two-component **Cu-2.**PF_6/(*tert*-Bu)Ph_2I^+ (0.3%/0.8% *w*/*w*) systems upon exposure to a LED at 405 nm (110 mW/cm^2) using (1) mechanosynthesized **Cu-2.**PF_6, (2) solution-synthesized **Cu-2**.BF_4, (3) using the three-component mechanosynthesized **Cu-2.**I/(*tert*-Bu)Ph_2I^+/Tin (II) (0.3%/0.8%/5% *w*/*w*/*w*) Reproduced with permission from the work in [104]. Copyright 2018 American Chemical Society.

Due to the strong ion pair interaction existing within **Cu-2.**I, this photoinitiator showed a lower photoinitiating ability than the two others (**Cu-2.**PF_6 or **Cu-2**.BF_4) so that its incorporation of **Cu-2.**I in the three-component system **Cu-2.**I/(*tert*-Bu)Ph_2I^+/Tin (II) (0.3%/0.8%/5% *w*/*w*/*w*) was required to reach

a final monomer conversion comparable to that obtained with **Cu-2**.PF_6 or **Cu-2**.BF_4 in two-component systems. Order of reactivity determined during the FRP of methacrylates was confirmed during the FRPCP of epoxides [104].

2.5. Green Approach towards the Synthesis of Copper-Based Redox and Photoredox Initiators of Polymerization

In 2018, mechanosynthesis was applied to the synthesis of photoinitiators activatable under near infrared light [69]. Indeed, on the basis of an interesting reaction discovered in 2016, where the grinding of copper (II) acetylacetonate ($Cu(acac)_2$ with 2-diphenylphosphinobenzoic acid (2-dppba) could give rise to a ligand exchange combined with a modification of the oxidation degree of Cu and the release of an acac• radical (see Figure 25) [70,71,120–122], this approach based on a redox reaction was named metal acetylacetonate–bidentate ligand interaction (MABLI). Optically, reaction between $Cu(acac)_2$ can be easily detected in solution, the initial blue solution turning green upon addition of 2-dppba. If originally, MABLI was developed to initiate redox polymerization, in 2018, this reaction was extended to photoactivated redox processes [67].

First, examination of the redox FRP of the UDMA/1,4-HPMA/1,4-BDMA blend with eight different complexes (**Cu-34**–**Cu-41**) (See Figures 26 and 27) revealed the **Cu-x (x = 34–41)**/2-dppba combinations to produce exothermic reactions. By monitoring the reaction process with a thermal imaging camera, an exothermicity ranging from 53 °C with **Cu-38** until 115 °C with **Cu-40** could be determined. Conversely, no reaction was observed with **Cu-41** [67]. Compared to the reference system 4-*N*, *N*-trimethylaniline (4-*N*,*N*-TMA)/benzoylperoxide (BPO), a significant reduction of the induction time could be observed with all complexes, corresponding to a 2-fold reduction (See Figure 27). However, based on the exothermicity of the reaction, similar monomer conversions can be expected with all systems.

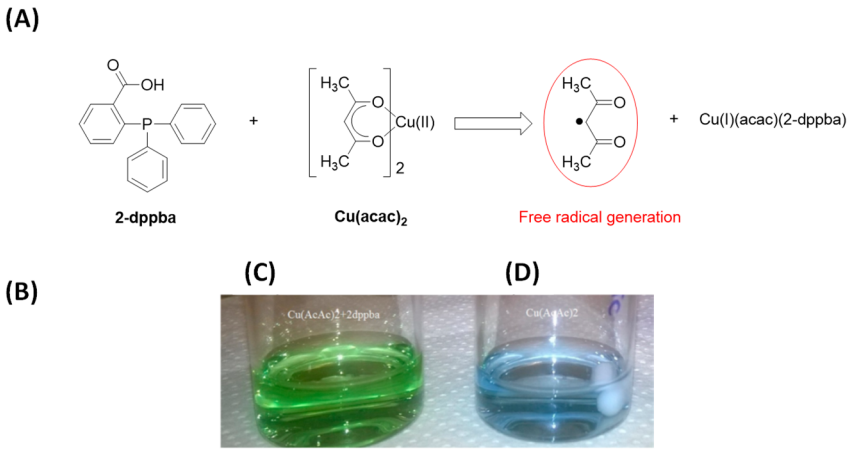

Figure 25. (**A**) Chemical mechanism involved in the metal acetylacetonate–bidentate ligand interaction (MABLI) process. (**B**) Evidence of the MABLI process in tetrahydrofuran (THF) solution. (**C**) Color of the solution after addition of 2-dppba to a $Cu(acac)_2$. (**D**) The same solution before addition. Reproduced with permission from the authors of [120]. Copyright 2016 American Chemical Society.

Interestingly, a marked chemical bleaching of the resins could be detected with five complexes (**Cu-34**–**Cu-37** and **Cu-40**). Coatings that were totally colorless could be obtained with **Cu-37** and **Cu-40**; these coatings are actively researched by industrials [123–125]. In fact, the higher the reactivity of the redox system was, the less colored the coating was. In light of the absorption spectra recorded in dichloromethane (see Figure 28), all complexes showed a broad absorption band extending over the visible range so that a photoactivation of the polymerization can also be obtained, upon addition of an iodonium salt to the initiating system. In this case, the coexistence of the redox and the photochemical mechanisms allow an efficient production of radicals, according to the mechanisms depicted in the Figure 29. Parallel to the formation of acac• radicals by ligand exchange with 2-dppba

(redox mechanism), the copper complex can also act as a photosensitizer, inducing the release of Ph• radicals by photodecomposition of the iodonium salt. As a result of this, the simultaneous formation of Ph• radicals and acac• radicals can efficiently accelerate the polymerization reaction. In the case of **Cu-35**–**Cu-38** and **Cu-41**, broad absorptions of the Cu (II) complexes enable these compounds to be activated at 405 or at 785 nm.

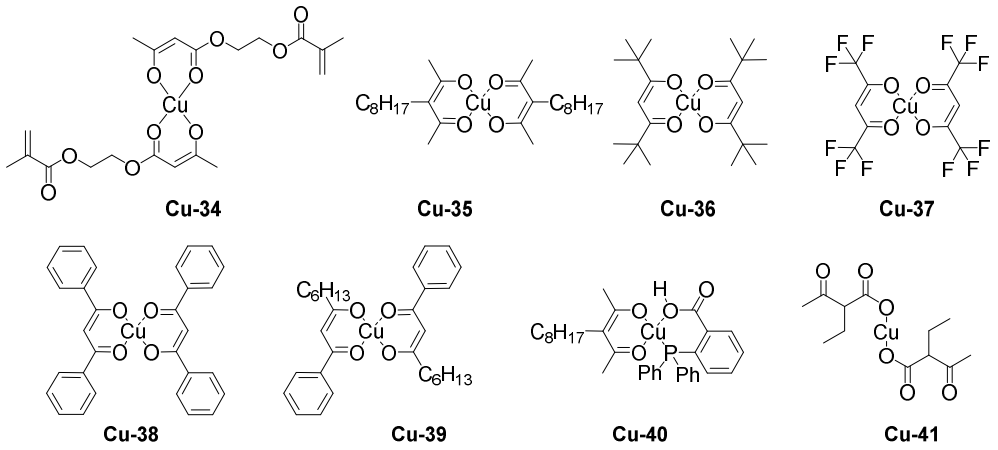

Figure 26. Chemical structures of copper complexes **Cu-34**–**Cu-41**.

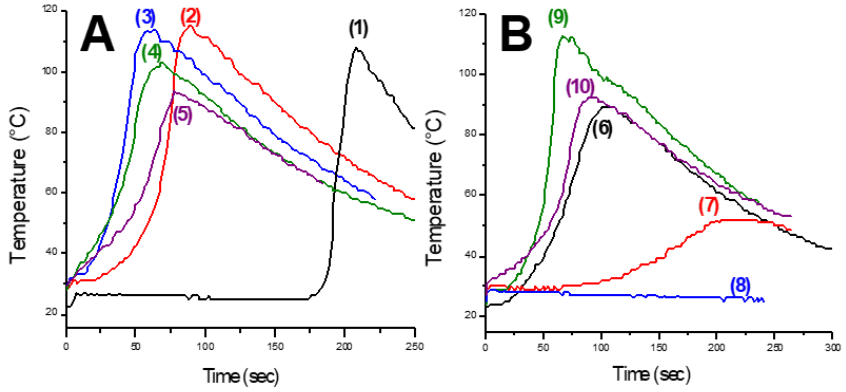

Figure 27. Optical pyrometric measurements under air for the redox polymerization of an UDMA/1,4-HPMA/1,4-BDMA blend using the two-component system **Cu-x (x = 34-41)**/2-dppba (1%/1.5%, *w*/*w*) (**A**). **(1)** Reference system 4-*N*,*N*-TMA/BPO (0.8%/1% *w*/*w*).**(2) Cu-40**. **(3) Cu-35**. **(4) Cu-36**. **(5) Cu-39**. (**B**). **(6)** $Cu(acac)_2$. **(7) Cu-38**. **(8) Cu-41**. **(9) Cu-37**. **(10) Cu-34**. Reproduced with permission from the authors of [67] Copyright 2018 The Royal Society of Chemistry.

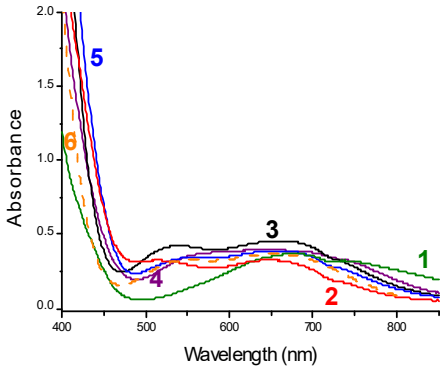

Figure 28. UV–visible absorption spectra of (1) **Cu-37** (2) **Cu-35** (3) **Cu-36** (4) **Cu-41** (5) **Cu-38** (6) **Cu(acac)$_2$**. Reproduced with permission from the authors of [67] Copyright 2018The Royal Society of Chemistry.

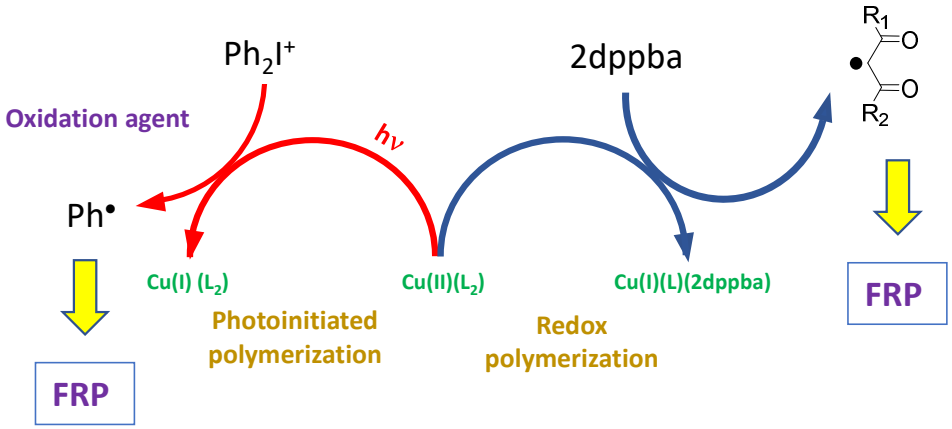

Figure 29. The dual source of radicals upon photoactivation of the redox process.

To evidence the advantages of light activation on the polymerization, tempol, which is a radical trapping agent, was added into the resins. As shown in Figure 30, benefits of the light activation for **Cu-37** (at 785 nm) or for **Cu-35** (at 405 nm or at 785 nm) could be clearly demonstrated, inducing a clear reduction of the reaction time while improving the final monomer conversions. Four-hundred-and-five nanometers and 785 nm were selected as the irradiation wavelengths in this study due to the panchromatic absorptions of **Cu-35**–**Cu-38** and **Cu-41**, so that photoactivation of the polymerization process is possible from the near-UV to the near-infrared range. Precisely, 405 nm was chosen as the first irradiation wavelength as this wavelength is currently under use in dentistry, notably for tooth filling and restoration. However, dental cements used to glue tooth structures such as crowns or bridges requires redox processes to be used as the light irradiation is not possible to chemically bond the different elements. To speed up the polymerization reaction, the redox process can be accelerated "on demand" by light irradiation, supporting the interest for (photo) redox polymerization processes. As far as the irradiation at 785 nm was concerned, a good light penetration can be obtained at long wavelength, as shown in the diagram presented in the Figure 1. The exceptional light penetration achievable at 785 nm can also be of interest for dental applications (filling of premolars and molars), but also for the polymerization of resins containing fillers [126–128]. By monitoring the C=C double bond conversion by Fourier transform infrared spectroscopy (FTIR), a two-fold reduction of the reaction time was obtained with **Cu-37** (37 s vs. 55 s without NIR light activation) with the two-component **Cu-37**/2-dppba/Iod (0.7%/1.5%/1.5% *w*/*w*/*w*) system. The most representative example of the light activation was obtained with **Cu-35**. Indeed, if no polymerization was detected with the two-component **Cu-37**/2-dppba/Iod (0.7%/1.5%/1.5% *w*/*w*/*w*) system in the presence of tempol (0.117 wt%), a monomer conversion of 40% could be obtained upon irradiation at 785 nm for 300 s and 62% upon irradiation at 405 nm (See Figure 29).

In fact, enhancement of the monomer conversion upon irradiation can be assigned to the coexistence of two initiating systems (the redox and the photochemical ones), generating a dual source of radicals upon photoexcitation (See Figure 28). However, as evidenced in the mechanism and as main drawback of this approach, the consumption of the copper complexes was irreversible [67].

Influence of the phosphine ligand used to release in situ acac• radicals by ligand exchange with $Cu(acac)_2$ was also examined and, in this aim, a series of nine phosphines was tested (see Figure 31) [120].

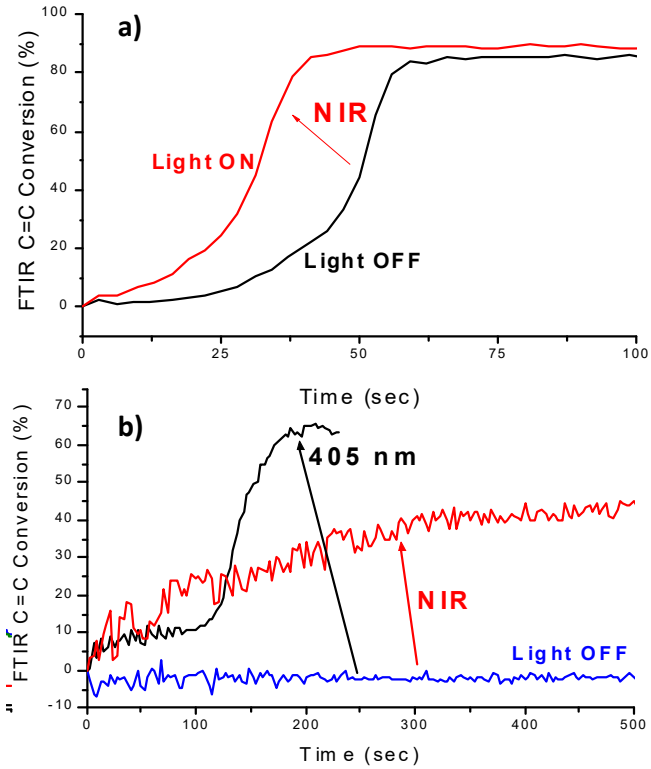

Figure 30. Final monomer conversions determined by real-time Fourier Transform Infrared Spectroscopy (RT-FTIR) measurements during the redox and redox photoactivated FRP under air. (**a**) With the two-component **Cu-37**/2-dppba/Iod (0.7%/1.5%/1.5% *w*/*w*/*w*) upon irradiation with a LED@785 nm (400 mW/cm^2) with 0.085 wt% tempol in the resin. (**b**) With the two-component **Cu-35**/2-dppba/Iod (0.7%/1.5%/1.5% *w*/*w*/*w*) upon irradiation with a LED@785 nm (400 mW/cm^2) or LED@405 nm (110 mW/cm^2) with 0.117 wt% tempol in the resin. Reproduced with permission from the authors of [67]. Copyright 2018 The Royal Society of Chemistry.

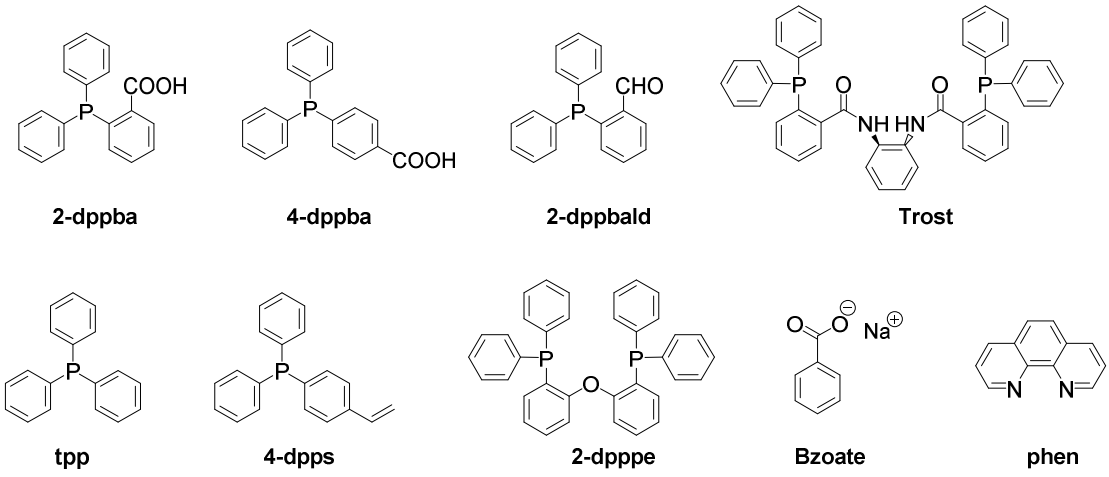

Figure 31. Chemical structures of phosphines used to initiate a ligand exchange with Cu(acac)$_2$.

In this work, the specific interaction existing between 2-dppba and Cu(acac)$_2$ was clearly evidenced. Indeed, neither 2-dppbald nor Trost ligand could induce a ligand exchange reaction, despite the presence of carbonyl groups in *ortho*-position of the phosphorus atom. A similar behavior was also observed with 4-dppba which is only an isomer of position of 2-dppba. While getting a deeper insight into the ligand exchange process occurring between 2-dppba and Cu(acac)$_2$, high-resolution mass spectrometry experiments revealed the formation of numerous products, some of them resulting from the oxidation

of the phosphine ligand by oxygen (see Figure 32) [120]. However, as previously mentioned during the FRP of the UDMA/1,4-HPMA/1,4-BDMA blend, a clear discoloration of the polymers during redox polymerization was observed. By analyzing the bulk polymer by TEM and SEM-EDX, formation of Cu(0) nanorods resulting from ligand decoordination could be demonstrated (see Figure 33). Especially, ligand release and reduction of Cu (II) to Cu (I) and then Cu(0) is facilitated by the exothermicity of the redox process.

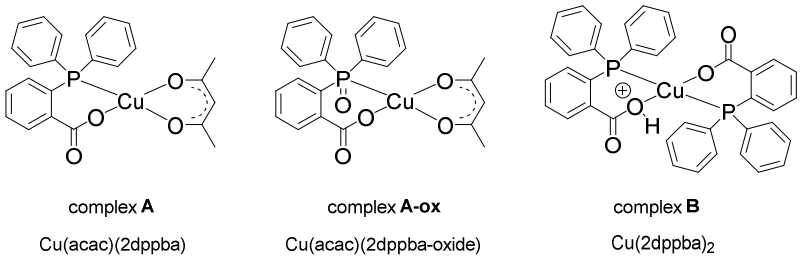

Figure 32. Chemical structures of copper complexes resulting from ligand exchange by 2-dppba with $Cu(acac)_2$.

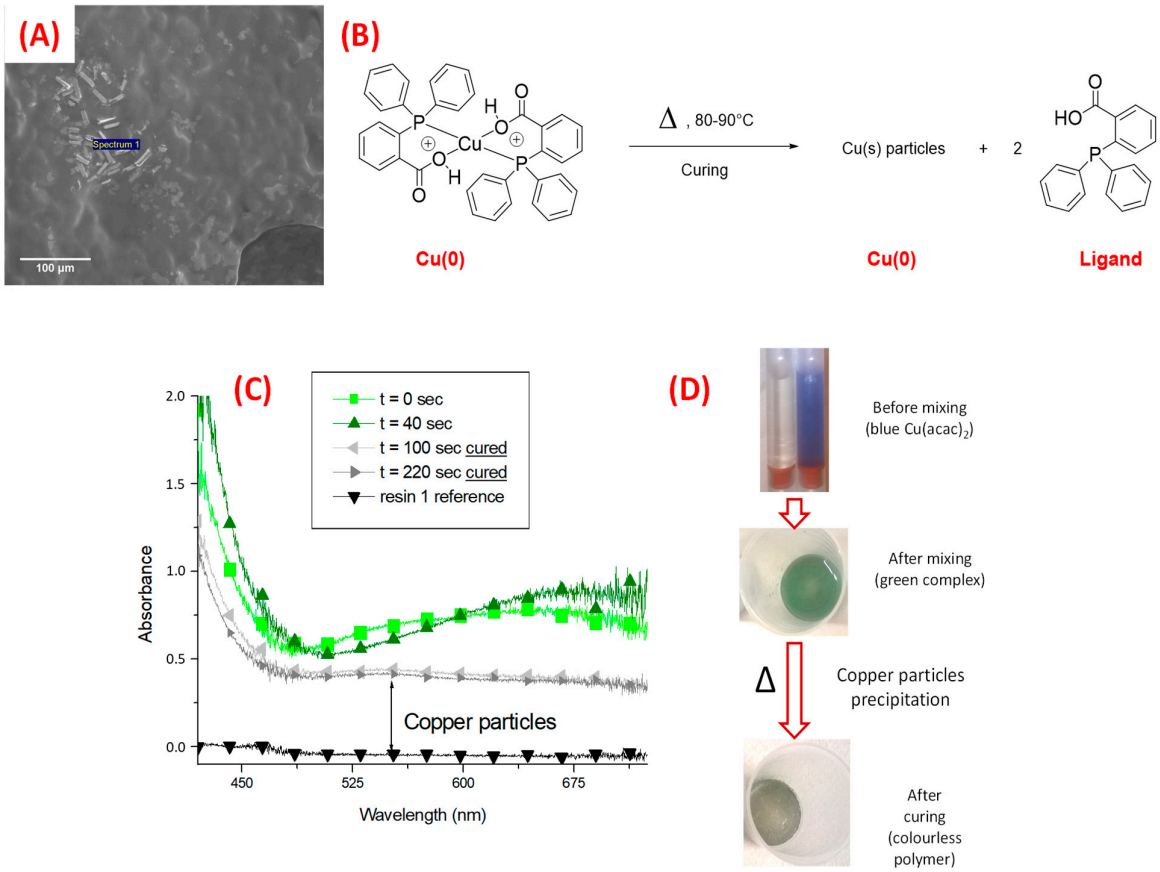

Figure 33. (**A**) SEM micrograph of the colorless polymer obtained by polymerization with the two-component system ($Cu(acac)_2$/2-dppba (2.2%/5.0% *w*/*w*) during the FRP of the UDMA/1,4-HPMA/1,4-BDMA blend. (**B**) Mechanism supporting the release of Cu(O) particles. (**C**) Monitoring the color change by UV-visible absorption spectroscopy (**D**) Color changes observed during the redox polymerizations of of the UDMA/1,4-HPMA/1,4-BDMA blend under air with the two-component system ($Cu(acac)_2$/2-dppba (0.32%/1.7% *w*/*w*). Reproduced with permission from the authors of [120]. Copyright 2016 The Royal Society of Chemistry.

In 2018, a breakthrough was achieved concerning the MABLI process [68]. Indeed, one of the major drawbacks of the initial concept of MABLI was the release of acac• radicals resulting in an irreversible consumption of the copper complex. In the updated version proposed in 2018, all components were changed. Thus, the three components of the initial initiating system ($Cu(acac)_2$/2-dppba/Ph_2I^+) were replaced by the following system ($Cu(Oct)_2$/Vit-C/BPO) where $Cu(Oct)_2$ stands for copper (II) 2-ethylhexanoate, Vit-C for vitamin-C and BPO for benzoyl peroxide. Using this approach, chemical integrity of the copper complex could be maintained during the redox polymerization, Ph(C = O)O• radicals being generated by decomposition of BPO. By means of vitamin C, the Cu (II) complex can also be regenerated so that the copper complex can be introduced in catalytic amount. By the appropriate choice of the reducing agent (i.e., vitamin C), this additive could also be used for the regeneration of the copper complex when engaged in a photochemical initiating system in the following combination $Cu(Oct)_2$/Vit-C/Iod. Therefore, a mechanism supporting the polymerization enhancement could be proposed for the photo (redox) polymerization with the four-component ($Cu(Oct)_2$/Vit-C/BPO/Iod) system (see Figure 34) [68].

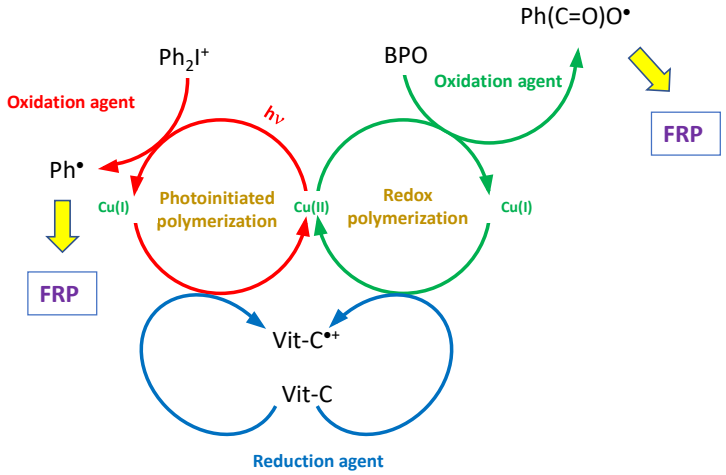

Figure 34. The two concomitant mechanisms involved in the photo (redox) polymerization with the four-component ($Cu(Oct)_2$/Vit-C/BPO/Iod) system upon photoexcitation of the curable resin.

The possibility to prepare interpenetrated polymer networks by copolymerization of a methacrylate/EPOX blend (50/50 *w/w*) was demonstrated, extending the scope of applicability of these redox processes to the CP of epoxides. If no improvement of the monomer conversion upon light activation was demonstrated, nevertheless, a significant enhancement of the final monomer conversion was observed, increasing from 75 to 95% for the methacrylate monomer while irradiating under at 405 nm (See Figure 35). The possibility to replace vitamin C by another reducing agent, i.e., tin (II) 2-ethylhexanoate was also demonstrated [68].

One of the key elements of the MABLI process is the generation of acac• radicals by successive ligand exchange with 2-dppba, resulting in turn in colorless coating due to Cu(0) nanoparticles precipitation (See Scheme 3) [68].

In 2017, mechanosynthesis of (Cu(acac) (2dppba)) **Cu-42** was reported and a comparison of the photoinitiation ability between the mechanosynthesized **Cu-42**, the solution-synthesized **Cu-42** and the two-component system $Cu(acac)_2$/2-dppba was established [69]. Interestingly, the grinding time was determined as being highly dependent of the quantities of reactant used. Thus, a grinding time varying between 2 min and 30 min was required to maximize the conversion of $Cu(acac)_2$ into **Cu-42** (see Figure 36), depending of the initial amount of the different reagents. By UV–visible absorption spectroscopy, a reduction of the molar extinction coefficient by ~30% compared to the solution, processes **Cu-42** was found, indicating the formation of byproducts by mechanochemistry.

Notably, due to an incomplete consumption of $Cu(acac)_2$, an influence on the polymerization profile of the (1,4-BDMA/HPMA/UDMA) blend could be detected (See Figure 37) [69].

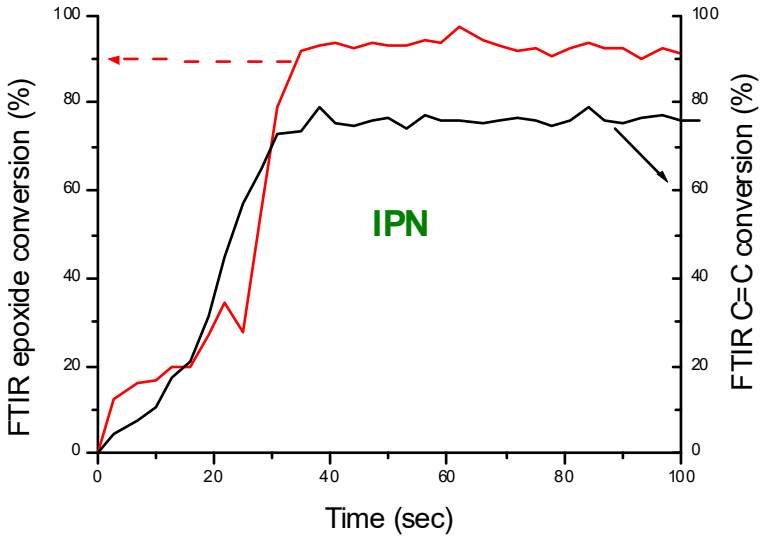

Figure 35. RT-FTIR monitoring of the polymerization of an EPOX/methacrylate mixture (1,4-BDMA/HPMA/UDMA) blend under air using the four component system ($Cu(Oct)_2$/BPO/Vit-C/Iod (0.75%/1.1%/1.5%/1%, *w*/*w*/*w*/*w*) with and without light irradiation at 405 nm. Reproduced with permission from the authors of [68]. Copyright 2018 The American Chemical Society.

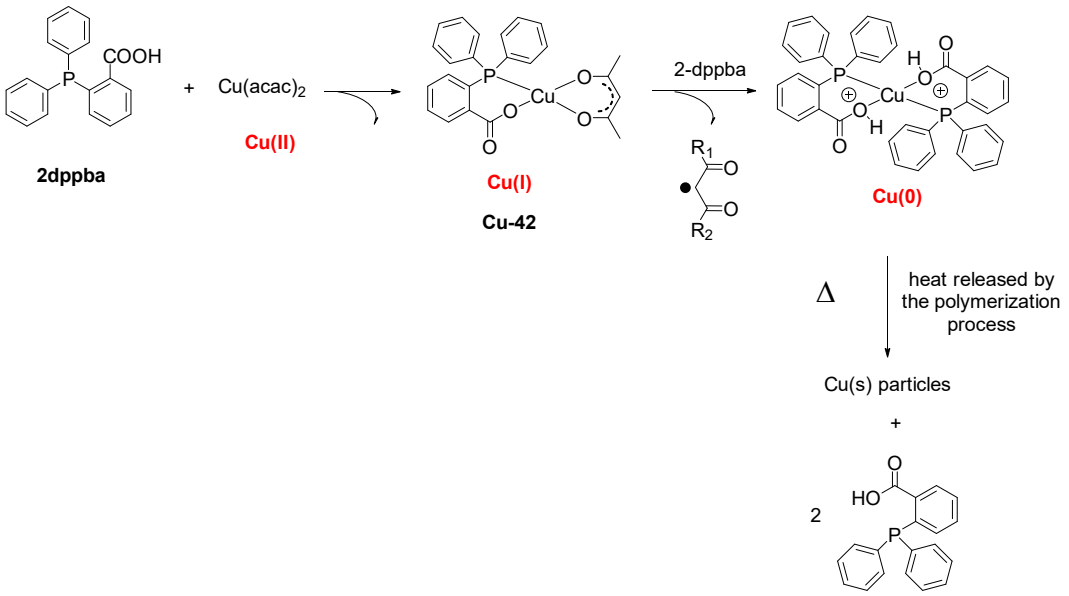

Scheme 3. Successive ligand exchange involved in the MABLI process.

Indeed, as shown in Figure 37, a faster polymerization process was found with the mechanosynthesized **Cu-42** during the FRP of the (1,4-BDMA/HPMA/UDMA) blend under air. Due to the presence of unreacted $Cu(acac)_2$ within the powder, a parallel reaction between $Cu(acac)_2$ and 2-dppba could occur, speeding up the polymerization kinetic [69]. Besides, similar final monomer conversions (81%) could be found with the two-component **Cu-42**/2-dppba (1%/1.5% *w*/*w*) systems, irrespective of the method used to prepare **Cu-42**. Conversely, due to the low solubility of $Cu(acac)_2$ in methacrylate resins, a lower final monomer conversion was determined, peaking at 68% after 120 s of reaction. Therefore, in light of the difference of solubility, **Cu-42** is from this point of view more interesting than $Cu(acac)_2$. As another topic of interest, almost colorless coatings could be obtained

with **Cu-42**, whereas a marked color could be detected for the polymer films prepared starting from $Cu(acac)_2$ [69].

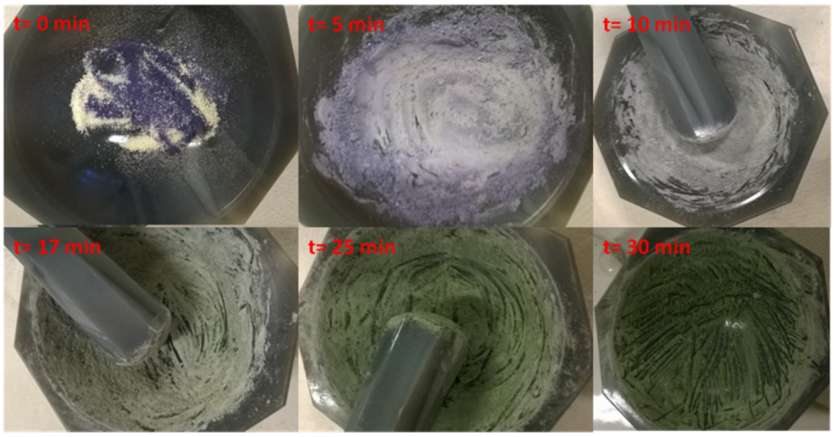

Figure 36. Monitoring of the synthesis of **Cu-42** over time. Reproduced with permission from the authors of [69]. Copyright 2017 John Wiley & Sons Ltd.

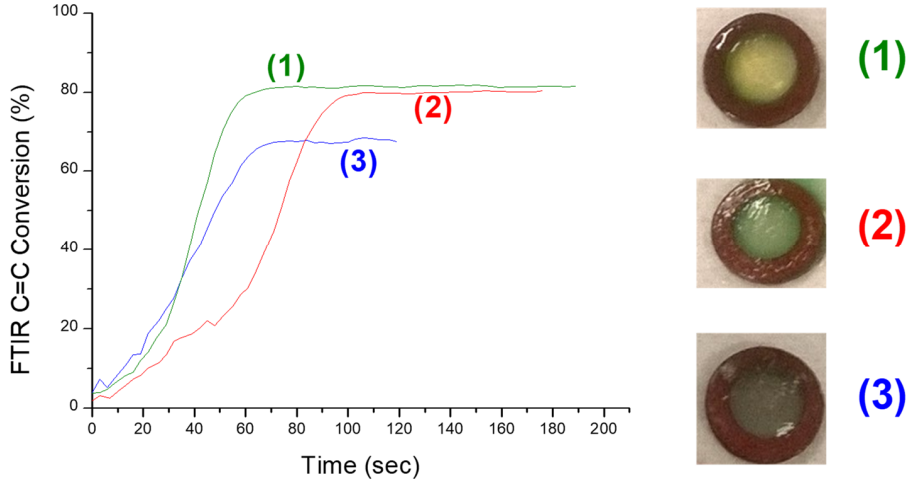

Figure 37. Polymerization profiles obtained during the FRP of the (1,4-BDMA/HPMA/UDMA) blend under air with the two-component **Cu-42**/2-dppba (1%/1.5% *w*/*w*) systems with **Cu-42** prepared **(1)**by mechanosynthesis **(2)**in solution **(3)**starting from $Cu(acac)_2$ and 2-dppba. Inset: pictures of the polymer films after polymerization. Reproduced with permission from the authors of [69]. Copyright 2017 John Wiley & Sons Ltd.

Finally, benefits of the photoactivation on the polymerization profiles of the three-component systems **Cu-42**/2-dppba/Iod (1%/1.8%/1.9% *w*/*w*/*w*) in the presence of 0.022 wt% tempol was clearly evidenced both at 405 and 785 nm (See Figure 38).

Thus, an increase of the monomer conversion from 20 to 60% within 100 s was obtained upon irradiation at 405 nm. A higher enhancement was determined at 785 nm since the monomer conversion increased from 23 to 70% upon light irradiation [69]. Additionally, due to a better light penetration within the resin at 785 nm, a complete bleaching of the polymer film was obtained. Technically, the combination of a redox and a photoactivated polymerization process is of crucial importance to get a homogeneous polymerization of the sample. Indeed, one advantage of photopolymerization process is its fast kinetics, enabling rapid polymerization of the surface of the sample and thus avoid oxygen diffusion. Conversely, due to the limited light penetration, the bottom part of the sample is always less polymerized than the top part. By contrast, redox polymerization allows an efficient curing of the bottom part of the sample, but oxygen inhibition adversely affect the monomer conversion at the

surface of the sample. Therefore, by combining the two approaches, a homogeneous polymerization over the whole sample can be expected (See Figure 39). In the present case, upon photoactivation of the polymerization process with the three-component system **Cu-42**/2-dppba/Iod (1%/1.8%/1.9% *w*/*w*/*w*) at 405 nm, the inhibition layer could be reduced from 23 to 15 µm during the FRP of the (1,4-BDMA/HPMA/UDMA) blend [69].

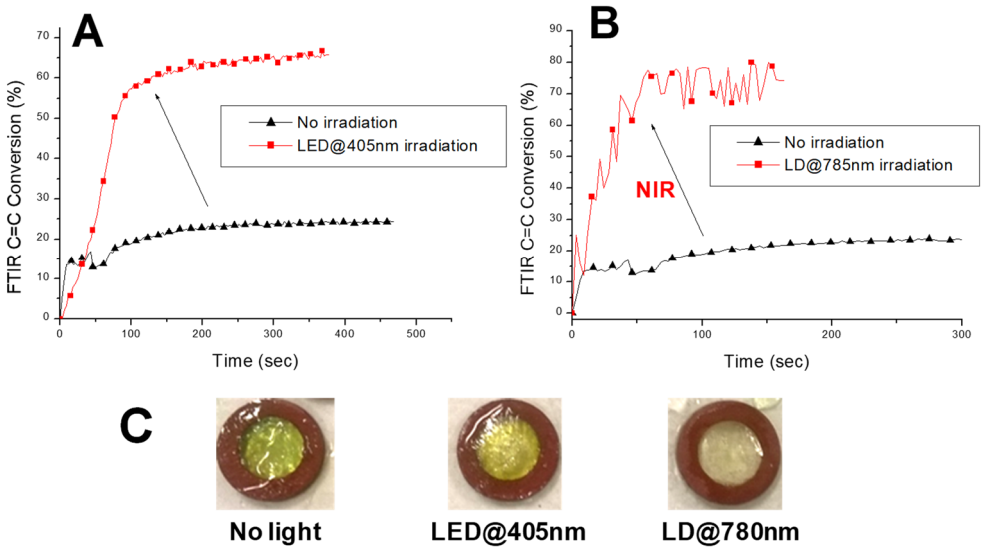

Figure 38. Polymerization profiles obtained during the FRP of the (1,4-BDMA/HPMA/UDMA) blend under air with the three-component systems **Cu-42**/2-dppba/Iod (1%/1.8%/1.9% *w*/*w*/*w*) (**A**) with and without light at 405 nm (**B**) with and without light irradiation at 785 nm. (**C**) Color of the photocurable resin before polymerization, after irradiation at 405 nm or after polymerization at 780 nm. Reproduced with permission from the authors of [69]. Copyright 2017 John Wiley & Sons Ltd.

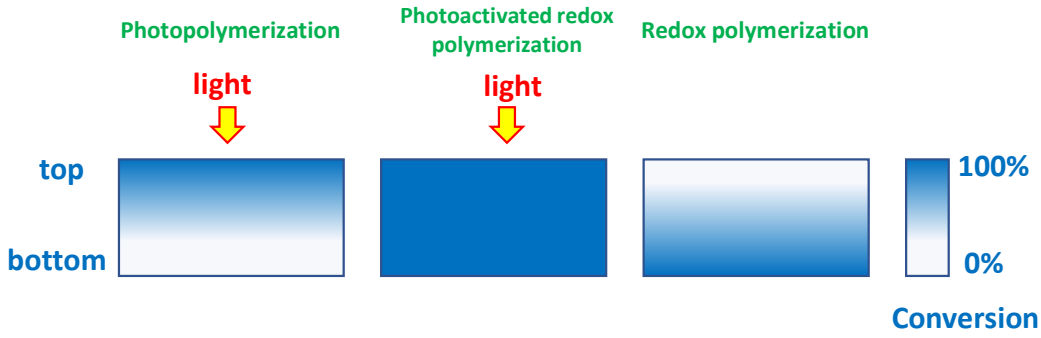

Figure 39. Specificities of photopolymerization, redox, and redox-activated polymerization.

2.6. Complexes with Elongated Excited State Lifetimes: The Basis of Chemical Engineering

As mentioned in the introduction section, a great deal of effort has been devoted to finely tune the excited state lifetimes of metal complexes. In this field, works of Chihaya Adachi on complexes exhibiting a Thermally Activated Delayed Fluorescence (TADF) property are remarkable and were mostly devoted to develop what can be called the third generation of emitters for Organic Light-Emitting Diodes [129–133]. The TADF property is not new; this property was reported for the first time in 1961 [134]. However, discrimination between a delayed fluorescence and a phosphorescence process could only be determined with accuracy in recent decades. To get such a property, an efficient strategy consists for purely organic compounds to isolate the electron-donating part from the electron-accepting part so that the electronic delocalization is drastically limited. A relevant example of this concerns 4-CzIPN, in which carbazole moieties have been introduced perpendicularly to the central core [135]. A few examples of such derivatives have notably been tested as photoinitiators of polymerization [136,137].

As far as metal complexes are concerned, the strategy is relatively similar, as substituents should be introduced so that the structural rearrangement in this excited state is not possible. As a result of this, an enhancement of the photoluminescence quantum yield combined with an elongation of the excited state lifetime can be obtained. With regards to photopolymerization, only the elongation of the excited state lifetime is of interest, as it ensures the photosensitizer to have more time to react in the excited state with the different additives. If the superiority of **Cu-4** over the other heteroleptic copper complexes was suspected to arise from this TADF property, no measurements evidencing that **Cu-4** was a TADF compound was provided. Benefits of the TADF property on the polymerization efficiency were given in 2018, with the comparison of **Cu-43** and **Cu-44** (see Figure 40) [138]. It has to be noticed that the photophysical properties of these two complexes have been examined prior to their uses in photopolymerization [139] As the main structural difference, **Cu-44** comprises two methyl groups at the inner position of phenanthroline ligand whereas no substituents are present on the ancillary ligand of **Cu-43**. From the absorption viewpoint, the absorption spectra of the two complexes are relatively similar in terms of molar extinction coefficients but also of absorption maxima (See Figure 41) [138]. Therefore, difference of photoinitiating ability could not originate from drastic difference of molar extinction coefficients. Conversely, drastic differences were found concerning their excited state lifetimes. Indeed, an enhancement from 0.02 µs for **Cu-43** to 2.5 µs for the sterically hindered **Cu-44** was determined, corresponding to a 100-fold elongation. Benefits of this elongation were immediately detected during the FRP of methacrylates or the FRPCP of epoxides upon irradiation with a LED at 405 nm under air. As shown in Figure 42 on the polymerization profiles of the BisGMA/TEGDMA blend or during the polymerization of EPOX, faster polymerization kinetics associated with higher final monomer conversions could be determined, evidencing the pertinence of the approach.

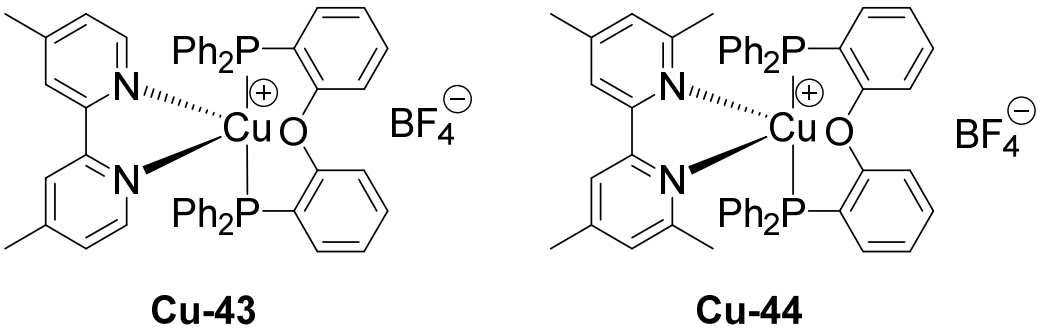

Figure 40. Chemical structures of **Cu-43** and **Cu-44**.

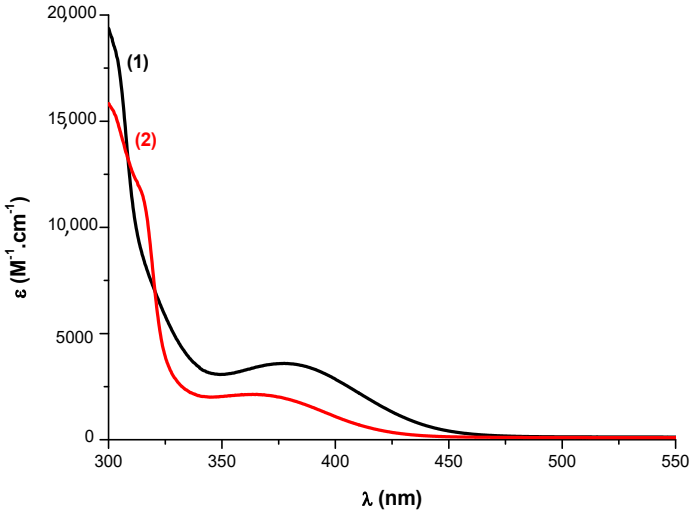

Figure 41. UV–visible absorption spectra of (1) **Cu-43** and (2) **Cu-44** in dichloromethane. Reproduced with permission from the authors of [138]. Copyright 2018 The Royal Society of Chemistry.

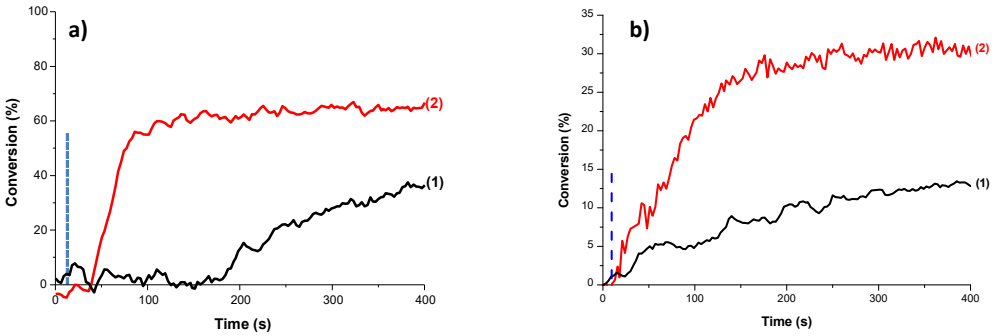

Figure 42. (**a**) Polymerization profiles obtained during the FRP of a BisGMA/TEGDMA blend in the presence of the two-component systems (1) **Cu-43**/Iod (0.5/1% *w*/*w*) and (2) **Cu-44**/Iod (0.5/1% *w*/*w*); (**b**) Photopolymerization profiles obtained during the FRPCP of EPOX in the presence of the three-component systems (1) **Cu-43**/Iod/NVK (0.5/1/1% *w*/*w*/*w*) and (2) **Cu-44**/Iod/NVK (0.5/1/1% *w*/*w*/*w*) upon irradiation with a LED at 405 nm (110 mW/cm^2). Reproduced with permission from the authors of [138], Copyright 2018 The Royal Society of Chemistry.

3. Conclusions

In this review, approximately 50 different copper complexes have been reported for their photoinitiating ability. As the initial uses of copper complexes for thermal atom transfer radical polymerizations (ATRP), great achievements have been obtained in photopolymerization. Concerning the milestones, the development of TADF-based photoinitiators has enabled to greatly improve the monomer conversion both during FRP and FRPCP processes due to the significant elongation of the excited state lifetime. In this field, by chemical engineering, **Cu-4** has been designed and synthesized and to the best of our knowledge can be cited as the most efficient copper-based photoinitiators at present. The number of publications only devoted to examine its photoinitiating ability attest of this. Parallel to photoassisted polymerization, copper complexes have been at the origin of a new redox polymerization technique named MABLI. Since the initial works in 2018, the photoassisted version or the catalytic version of MABLI has been proposed, paving the way towards future developments in this field. Another advantage of copper complexes relies in the possibility to prepare these complexes by mechanochemistry and copper complexes are at the forefront of the research concerning the mechanosynthesis of (photo) initiators of polymerization. In light of these three axes of research, the development of novel copper-based photoinitiators is ensured in the Future.

Author Contributions: Conceptualization, G.N. and F.D.; methodology, G.N. and F.D.; validation, G.N. and F.D.; investigation, G.N. and F.D.; resources, F.D.; data curation, F.D.; writing—original draft preparation, G.N. and F.D.; writing—review and editing, G.N. and F.D.; supervision, G.N. and F.D.; project administration, F.D.; funding acquisition, F.D. All authors have read and agreed to the published version of the manuscript.

Funding: The authors thank Aix Marseille University (AMU) and the Centre National de la Recherche Scientifique (CNRS) for their financial support. The Agence Nationale de la Recherche (ANR agency) is acknowledged for its financial support through the PhD grant of Guillaume Noirbent (ANR-17-CE08-0054 VISICAT project).

Acknowledgments: The authors thank Aix Marseille University (AMU) and the Centre National de la Recherche Scientifique (CNRS) for their financial support.

Conflicts of Interest: The authors declare no conflict of interest.

References

1. Jasinski, F.; Zetterlund, P.B.; Braun, A.M.; Chemtob, A. Photopolymerization in dispersed systems. *Prog. Polym. Sci.* **2018**, *84*, 47–88. [CrossRef]
2. Ng, G.; Yeow, J.; Xu, J.; Boyer, C. Application of oxygen tolerant PET-RAFT to polymerization-induced self-assembly. *Polym. Chem.* **2017**, *8*, 2841–2851. [CrossRef]
3. Pan, X.; Tasdelen, M.A.; Laun, J.; Junkers, T.; Yagci, Y.; Matyjaszewski, K. Photomediated controlled radical polymerization. *Prog. Polym. Sci.* **2016**, *62*, 73–125. [CrossRef]

4. Abdallah, M.; Hijazi, A.; Dumur, F.; Lalevée, J. Coumarins as powerful photosensitizers for the cationic polymerization of epoxy-silicones under near-UV and visible light and applications for 3D printing technology. *Molecules* **2020**, *25*, 2063. [CrossRef]
5. Noè, C.; Malburet, S.; Bouvet-Marchand, A.; Graillot, A.; Loubat, C.; Sangermano, M. Cationic photopolymerization of bio-renewable epoxidized monomers. *Prog. Org. Coat.* **2019**, *133*, 131–138. [CrossRef]
6. Lalevée, J.; Mokbel, H.; Fouassier, J.-P. Recent developments of versatile photoinitiating systems for cationic ring opening polymerization operating at any wavelengths and under low light intensity sources. *Molecules* **2015**, *20*, 7201–7221. [CrossRef] [PubMed]
7. Zhang, Z.; Corrigan, N.; Bagheri, A.; Jin, J.; Boyer, C. A versatile 3D and 4D printing system through photocontrolled raft polymerization. *Angew. Chem.* **2019**, *131*, 18122–18131. [CrossRef]
8. Lee, A.Y.; An, J.; Chua, C.K. Two-way 4D-printing: A review on the reversibility of 3d-printed shape memory materials. *Engineering* **2017**, *3*, 663–674. [CrossRef]
9. Bagheri, A.; Jin, J. Photopolymerization in 3D Printing. *ACS Appl. Polym. Mat.* **2019**, *1*, 593–611. [CrossRef]
10. Aduba, D.C., Jr.; Margaretta, E.D.; Marnot, A.E.C.; Heifferon, K.V.; Surbey, W.R.; Chartrain, N.A.; Whittington, A.R.; Long, T.E.; Williams, C.B. Vat photopolymerization 3D printing of acid-cleavable PEG-methacrylate networks for biomaterial applications. *Mat. Today Commun.* **2019**, *19*, 204–211. [CrossRef]
11. Mendes-Felipe, C.; Oliveira, J.; Etxebarria, I.; Vilas-Vilela, J.L.; Lanceros-Mendez, S. State-of-the-Art and Future Challenges of UV Curable Polymer-Based Smart Materials for Printing Technologies. *Adv. Mat. Technol.* **2019**, *4*, 1800618. [CrossRef]
12. Yagci, Y.; Jockusch, S.; Turro, N.J. Photoinitiated Polymerization: Advances, Challenges, and Opportunities. *Macromolecules* **2010**, *43*, 6245–6260. [CrossRef]
13. Shao, J.; Huang, Y.; Fan, Q. Visible light initiating systems for photopolymerization: Status, development and challenges. *Polym. Chem.* **2014**, *5*, 4195–4210. [CrossRef]
14. Dietlin, C.; Schweizer, S.; Xiao, P.; Zhang, J.; Morlet-Savary, F.; Graff, B.; Fouassier, J.P.; Lalevée, J. Photopolymerization upon LEDs: New photoinitiating systems and strategies. *Polym. Chem.* **2015**, *6*, 3895–3912. [CrossRef]
15. Ibrahim-Ouali, M.; Dumur, F. Recent advances on metal-based near-infrared and infrared emitting OLEDs. *Molecules* **2019**, *24*, 1412. [CrossRef] [PubMed]
16. Dumur, F. Zinc complexes in OLEDs: An overview. *Synth. Met.* **2014**, *195*, 241–251. [CrossRef]
17. Dumur, F. Recent advances in organic light-emitting devices comprising copper complexes: A realistic approach for low-cost and highly emissive devices? *Org. Electron.* **2015**, *21*, 27–39. [CrossRef]
18. Yoshino, F.; Yoshida, A. Effects of blue-light irradiation during dental treatment. *Jap. Dent. Sci. Rev.* **2018**, *54*, 160–168. [CrossRef]
19. Khairunisah Ghazali, S.; Syaimima Syaiful Azim, F.; Adrus, N.; Jamaluddin, J. The Effectiveness of UV-LED Photopolymerisation over Conventional UV-Mercury for Polyurethane Acrylate Coating. *J. Photopolym. Sci. Technol.* **2019**, *32*, 705–710. [CrossRef]
20. Xiao, P.; Zhang, J.; Dumur, F.; Tehfe, M.-A.; Morlet-Savary, F.; Graff, B.; Gigmes, D.; Fouassier, J.-P.; Lalevée, J. Photoinitiating systems: Recent progress in visible light induced cationic and radical photopolymerization reactions under soft conditions. *Prog. Polym. Sci.* **2015**, *41*, 32–66. [CrossRef]
21. Bonardi, A.H.; Dumur, F.; Grant, T.M.; Noirbent, G.; Gigmes, D.; Lessard, B.H.; Fouassier, J.-P.; Lalevée, J. High performance near infrared (NIR) photoinitiating systems operating under low light intensity and in presence of oxygen. *Macromolecules* **2018**, *51*, 1314–1324. [CrossRef]
22. Garra, P.; Dietlin, C.; Morlet-Savary, F.; Dumur, F.; Gigmes, D.; Fouassier, J.-P.; Lalevée, J. Photopolymerization processes of thick films and in shadow areas: A review for the access to composites. *Polym. Chem.* **2017**, *8*, 7088–7101. [CrossRef]
23. Dumur, F. Recent advances on carbazole-based photoinitiators of polymerization. *Eur. Polym. J.* **2020**, *125*, 109503. [CrossRef]
24. Dumur, F. Recent advances on pyrene-based photoinitiators of polymerization. *Eur. Polym. J.* **2020**, *126*, 109564. [CrossRef]
25. Noirbent, G.; Dumur, F. Recent advances on naphthalic anhydrides and 1,8-naphthalimide-based photoinitiators of polymerization. *Eur. Polym. J.* **2020**, *132*, 109702. [CrossRef]

26. Pigot, C.; Noirbent, G.; Brunel, D.; Dumur, F. Recent advances on push-pull organic dyes as visible light photoinitiators of polymerization. *Eur. Polym. J.* **2020**, *133*, 109797. [CrossRef]
27. Tehfe, M.-A.; Dumur, F.; Graff, B.; Gigmes, D.; Fouassier, J.-P.; Lalevée, J. Blue-to-red light sensitive push-pull structured photoinitiators: Indanedione derivatives for radical and cationic photopolymerization reactions. *Macromolecules* **2013**, *46*, 3332–3341. [CrossRef]
28. Tehfe, M.-A.; Dumur, F.; Graff, B.; Morlet-Savary, F.; Gigmes, D.; Fouassier, J.-P.; Lalevée, J. New push-pull dyes derived from Michler's ketone for polymerization reactions upon visible lights. *Macromolecules* **2013**, *46*, 3761–3770. [CrossRef]
29. Tehfe, M.-A.; Dumur, F.; Graff, B.; Morlet-Savary, F.; Gigmes, D.; Fouassier, J.-P.; Lalevée, J. Push-pull (thio)barbituric acid derivatives in dye photosensitized radical and cationic polymerization reactions under 457/473 nm Laser beams or blue LEDs. *Polym. Chem.* **2013**, *4*, 3866–3875. [CrossRef]
30. Mokbel, H.; Telitel, S.; Dumur, F.; Vidal, L.; Versace, D.-L.; Tehfe, M.-A.; Graff, B.; Toufaily, J.; Fouassier, J.-P.; Gigmes, D.; et al. Photoinitiating systems of polymerization and in-situ incorporation of metal nanoparticles in polymer matrixes upon visible lights: Push-pull malonate and malonitrile based dyes. *Polym. Chem.* **2013**, *4*, 5679–5687. [CrossRef]
31. Xiao, P.; Frigoli, M.; Dumur, F.; Graff, B.; Gigmes, D.; Fouassier, J.-P.; Lalevée, J. Julolidine or fluorenone based push-pull dyes for polymerization upon soft polychromatic visible light or green light. *Macromolecules* **2014**, *47*, 106–112. [CrossRef]
32. Sun, K.; Pigot, C.; Chen, H.; Nechab, M.; Gigmes, D.; Morlet-Savary, F.; Graff, B.; Liu, S.; Xiao, P.; Dumur, F.; et al. Free radical photopolymerization and 3D printing using newly developed dyes: Indane-1,3-dione and 1*H*-cyclopentanaphthalene-1,3-dione derivatives as photoinitiators in three-component systems. *Catalysts* **2020**, *10*, 463. [CrossRef]
33. Xiao, P.; Dumur, F.; Graff, B.; Vidal, L.; Gigmes, D.; Fouassier, J.-P.; Lalevée, J. Structural effects in the indanedione skeleton for the design of low intensity 300-500 nm light sensitive initiators. *Macromolecules* **2014**, *47*, 26–34. [CrossRef]
34. Xiao, P.; Dumur, F.; Graff, B.; Fouassier, J.-P.; Gigmes, D.; Lalevée, J. Cationic and thiol-ene photopolymerization upon red lights using anthraquinone derivatives as photoinitiators. *Macromolecules* **2013**, *46*, 6744–6750. [CrossRef]
35. Dumur, F.; Gigmes, D.; Fouassier, J.-P.; Lalevée, J. Organic Electronics: An El Dorado in the quest of new photocatalysts as photoinitiators of polymerization. *Acc. Chem. Res.* **2016**, *49*, 1980–1989. [CrossRef]
36. Xiao, P.; Dumur, F.; Tehfe, M.-A.; Gigmes, D.; Fouassier, J.-P.; Lalevée, J. Red-light-induced cationic photopolymerization: Perylene derivatives as efficient photoinitiators. *Macromol. Rapid. Commun.* **2013**, *34*, 1452–1458. [CrossRef]
37. Lalevée, J.; Peter, M.; Dumur, F.; Gigmes, D.; Blanchard, N.; Tehfe, M.-A.; Morlet-Savary, F.; Fouassier, J.-P. Subtle ligand effects in oxidative photocatalysis with iridium complexes: Application to photopolymerization. *Chem. Eur. J.* **2011**, *17*, 15027–15031. [CrossRef]
38. Lalevée, J.; Tehfe, M.-A.; Dumur, F.; Gigmes, D.; Blanchard, N.; Morlet-Savary, F.; Fouassier, J.-P. Iridium photocatalysts in free radical photopolymerization under visible lights. *ACS Macro Lett.* **2012**, *1*, 286–290. [CrossRef]
39. Lalevée, J.; Dumur, F.; Mayer, C.R.; Gigmes, D.; Nasr, G.; Tehfe, M.-A.; Telitel, S.; Morlet-Savary, F.; Graff, B.; Fouassier, J.-P. Photopolymerization of *N*-vinylcarbazole using visible-light harvesting iridium complexes as photoinitiators. *Macromolecules* **2012**, *45*, 4134–4141. [CrossRef]
40. Telitel, S.; Dumur, F.; Telitel, S.; Soppera, O.; Lepeltier, M.; Guillaneuf, Y.; Poly, J.; Morlet-Savary, F.; Fioux, P.; Fouassier, J.-P.; et al. Photoredox catalysis using a new iridium complex as an efficient toolbox for radical, cationic and controlled polymerizations under soft blue to green lights. *Polym. Chem.* **2015**, *6*, 613–624. [CrossRef]
41. Telitel, S.; Dumur, F.; Lepeltier, M.; Gigmes, D.; Fouassier, J.-P.; Lalevée, J. Photoredox process induced polymerization reactions: Iridium complexes for panchromatic photoinitiating systems. *C. R. Chimie* **2016**, *19*, 71–78. [CrossRef]
42. Tehfe, M.-A.; Lepeltier, M.; Dumur, F.; Gigmes, D.; Fouassier, J.-P.; Lalevée, J. Structural effects in the iridium complex series: Photoredox catalysis and photoinitiation of polymerization reactions under visible lights. *Macromol. Chem. Phys.* **2017**, *218*, 1700192. [CrossRef]

43. Tehfe, M.-A.; Lalevée, J.; Dumur, F.; Telitel, S.; Gigmes, D.; Contal, E.; Bertin, D.; Fouassier, J.-P. Zinc-based metal complexes as new photocatalysts in polymerization initiating systems. *Eur. Polym. J.* **2013**, *49*, 1040–1049. [CrossRef]
44. Versace, D.-L.; Bourgon, J.; Leroy, E.; Dumur, F.; Gigmes, D.; Fouassier, J.-P.; Lalevée, J. Zinc complex based photoinitiating systems for acrylate polymerization under air; in situ formation of Zn-based fillers and composites. *Polym. Chem.* **2014**, *5*, 6569–6576. [CrossRef]
45. Al Mousawi, A.; Poriel, C.; Dumur, F.; Toufaily, J.; Hamieh, T.; Fouassier, J.-P.; Lalevée, J. Zinc tetraphenylporphyrin as high performance visible-light photoinitiator of cationic photosensitive resins for LED projector 3D printing applications. *Macromolecules* **2017**, *50*, 746–753. [CrossRef]
46. Zhang, J.; Campolo, D.; Dumur, F.; Xiao, P.; Fouassier, J.-P.; Gigmes, D.; Lalevée, J. Iron complexes as photoinitiators for radical and cationic polymerization through photoredox catalysis processes. *J. Polym. Sci. A Polym. Chem.* **2015**, *53*, 42–49. [CrossRef]
47. Xiao, P.; Zhang, J.; Campolo, D.; Dumur, F.; Gigmes, D.; Fouassier, J.-P.; Lalevée, J. Copper and iron complexes as visible-light-sensitive photoinitiators of polymerization. *J. Polym. Sci. A Polym. Chem.* **2015**, *53*, 2673–2684. [CrossRef]
48. Telitel, S.; Dumur, F.; Campolo, D.; Poly, J.; Gigmes, D.; Fouassier, J.-P.; Lalevée, J. Iron complexes as potential photocatalysts for controlled radical photopolymerizations: A tool for modifications and patterning of surfaces. *J. Polym. Sci. A Polym. Chem.* **2016**, *54*, 702–713. [CrossRef]
49. Zhang, J.; Campolo, D.; Dumur, F.; Xiao, P.; Fouassier, J.-P.; Gigmes, D.; Lalevée, J. Visible-light-sensitive photoredox catalysis by iron complexes: Applications in cationic and radical polymerization reactions. *J. Polym. Sci. A Polym. Chem.* **2016**, *54*, 2247–2253. [CrossRef]
50. Zhang, J.; Campolo, D.; Dumur, F.; Xiao, P.; Fouassier, J.-P.; Gigmes, D.; Lalevée, J. Novel iron complexes in visible-light-sensitive photoredox catalysis: Effect of ligands on their photoinitiation efficiencies. *ChemCatChem* **2016**, *8*, 2227–2233. [CrossRef]
51. Di Bernardo, P.; Zanonato, P.L.; Tamburini, S.; Tomasin, P.; Vigato, P.A. Complexation behaviour and stability of Schiff bases in aqueous solution. The case of an acyclic diimino(amino) diphenol and its reduced triamine derivative. *Dalton Trans.* **2006**, *39*, 4711–4721. [CrossRef] [PubMed]
52. Garra, P.; Brunel, D.; Noirbent, G.; Graff, B.; Morlet-Savary, F.; Dietlin, C.; Sidorkin, V.F.; Dumur, F.; Duché, D.; Gigmes, D.; et al. Ferrocene-based (photo)redox polymerization under long wavelengths. *Polym. Chem.* **2019**, *10*, 1431–1441. [CrossRef]
53. Brunel, D.; Noirbent, G.; Dumur, F. Ferrocene: An unrivaled electroactive building block for the design of push-pull dyes with near-infrared and infrared absorptions. *Dyes Pigm.* **2019**, *170*, 107611. [CrossRef]
54. Cuttell, D.G.; Kuang, S.-M.; Fanwick, P.E.; McMillin, D.R.; Walton, R.A. Simple Cu(I) Complexes with Unprecedented Excited-State Lifetimes. *J. Am. Chem. Soc.* **2002**, *124*, 6–7. [CrossRef]
55. Zhang, Q.; Zhou, Q.; Cheng, Y.; Wang, L.; Ma, D.; Jing, X.; Wang, F. Highly efficient electroluminescence from green-light-emitting electrochemical cells based on CuI complexes. *Adv. Funct. Mat.* **2006**, *16*, 1203–1208. [CrossRef]
56. Zhang, Q.; Komino, T.; Huang, S.; Matsunami, S.; Goushi, K.; Adachi, C. Triplet exciton confinement in green organic light-emitting diodes containing luminescent charge-transfer Cu(I) complexes. *Adv. Funct. Mat.* **2012**, *22*, 2327–2336. [CrossRef]
57. Armaroli, N.; Accorsi, G.; Holler, M.; Moudam, O.; Nierengarten, J.F.; Zhou, Z.; Wegh, R.T.; Welter, R. Highly luminescent CuI complexes for light-emitting electrochemical cells. *Adv. Mat.* **2006**, *18*, 1313–1316. [CrossRef]
58. Hernandez-Perez, A.C.; Vlassova, A.; Collins, S.K. Toward a visible light mediated photocyclization: Cu-based sensitizers for the synthesis of [5]helicene. *Org. Lett.* **2012**, *14*, 2988–2991. [CrossRef]
59. Pirtsch, M.; Paria, S.; Matsuno, T.; Isobe, H.; Reiser, O. [Cu(dap)$_2$Cl] as an efficient visible-light-driven photoredox catalyst in carbon–carbon bond-forming reactions. *Chem. Eur. J.* **2012**, *18*, 7336–7340. [CrossRef]
60. Gong, T.; Adzima, B.J.; Baker, N.H.; Bowman, C.N. Photopolymerization reactions using the photoinitiated copper (I)-catalyzed azide-alkyne cycloaddition (CuAAC) reaction. *Adv. Mat.* **2013**, *25*, 2024–2028. [CrossRef]
61. Alzahrani, A.A.; Erbse, A.H.; Bowman, C.N. Evaluation and development of novel photoinitiator complexes for photoinitiating the copper-catalyzed azide-alkyne cycloaddition reaction. *Polym. Chem.* **2014**, *5*, 1874–1882. [CrossRef]

62. Xiao, P.; Dumur, F.; Zhang, J.; Fouassier, J.-P.; Gigmes, D.; Lalevée, J. Copper complexes in radical photoinitiating systems: Applications to free radical and cationic polymerization under visible lights. *Macromolecules* **2014**, *47*, 3837–3844. [CrossRef]
63. Poli, R.; Allan, L.E.N.; Shaver, M.P. Iron-mediated reversible deactivation controlled radical polymerization. *Prog. Polym. Sci.* **2014**, *39*, 1827–1845. [CrossRef]
64. Wang, J.S.; Matyjaszewski, K. Controlled/"living" radical polymerization atom transfer radical polymerization in the presence of transition-metal complexes. *J. Am. Chem. Soc.* **1995**, *117*, 5614–5615. [CrossRef]
65. Kamigaito, M.; Ando, T.; Sawamoto, M. Metal-catalyzed living radical polymerization. *Chem. Rev.* **2001**, *101*, 3689–3746. [CrossRef]
66. Cunningham, A.F.; Desobry, V. *Radiation Curing in Polymer Science and Technology*; Fouassier, J.-P., Rabek, J.-F., Eds.; Elsevier: Barking, UK, 1993; Volume 2, pp. 323–374.
67. Garra, P.; Dumur, F.; Nechab, M.; Morlet-Savary, F.; Dietlin, C.; Graff, B.; Gigmes, D.; Fouassier, J.P.; Lalevée, J. Stable copper acetylacetonate-based oxidizing agents in redox (NIR photoactivated) polymerization: An opportunity for the one pot grafting from approach and an example on a 3D printed object. *Polym. Chem.* **2018**, *9*, 2173–2182. [CrossRef]
68. Garra, P.; Carré, M.; Dumur, F.; Morlet-Savary, F.; Dietlin, C.; Gigmes, D.; Fouassier, J.P.; Lalevée, J. Copper-based (photo)redox initiating systems as highly efficient systems for interpenetrating polymer network preparation. *Macromolecules* **2018**, *51*, 679–688. [CrossRef]
69. Garra, P.; Dumur, F.; Morlet-Savary, F.; Dietlin, C.; Gigmes, D.; Fouassier, J.P.; Lalevée, J. Mechanosynthesis of a copper complex for redox initiating systems with a unique near infrared light activation. *J. Polym. Sci. A Polym. Chem.* **2017**, *55*, 3646–3655. [CrossRef]
70. Garra, P.; Morlet-Savary, F.; Graff, B.; Dumur, F.; Monnier, V.; Dietlin, C.; Gigmes, D.; Fouassier, J.P.; Lalevée, J. Metal acetylacetonate-bidentate ligand interaction (MABLI) as highly efficient free radical generating systems for polymer synthesis. *Polym. Chem.* **2018**, *9*, 1371–1378. [CrossRef]
71. Garra, P.; Dumur, F.; Gigmes, D.; Nechab, M.; Morlet-Savary, F.; Dietlin, C.; Gree, S.; Fouassier, J.P.; Lalevée, J. Metal acetylacetonate-bidentate ligand interaction (MABLI) (photo)activated polymerization: Toward high performance amine-free, peroxide-free redox radical (photo)initiating systems. *Macromolecules* **2018**, *51*, 2706–2715. [CrossRef]
72. Dumur, F.; Bertin, D.; Gigmes, D. Iridium (III) complexes as promising emitters for solid-state light-emitting electrochemical cells (LECs). *Int. J. Nanotechnol.* **2012**, *9*, 377–395. [CrossRef]
73. Dumur, F.; Contal, E.; Wantz, G.; Gigmes, D. Photoluminescence of zinc complexes: Easily tunable optical properties by the bridge between the imido groups of Schiff-base ligands. *Eur. J. Inorg. Chem.* **2014**, 4186–4198. [CrossRef]
74. Villotte, S.; Gigmes, D.; Dumur, F.; Lalevée, J. Design of iodonium salts for UV or near-UV LEDs for photoacid generator and polymerization purposes. *Molecules* **2020**, *25*, 149. [CrossRef] [PubMed]
75. Sakai, Y.; Sagara, Y.; Nomura, H.; Nakamura, N.; Suzuki, Y.; Miyazaki, H.; Adachi, C. Zinc complexes exhibiting highly efficient thermally activated delayed fluorescence and their application to organic light-emitting diodes. *Chem. Commun.* **2015**, *51*, 3181–3184. [CrossRef] [PubMed]
76. Uoyama, H.; Goushi, K.; Shizu, K.; Nomura, H.; Adachi, C. Highly efficient organic light-emitting diodes from delayed fluorescence. *Nature* **2012**, *492*, 234–238. [CrossRef]
77. Atkins, C.E.; Park, S.E.; Blaszak, J.A.; McMillin, D.R. A two-level approach to deconvoluting absorbance data involving multiple species. Applications to copper systems. *Inorg. Chem.* **1984**, *23*, 569–572. [CrossRef]
78. Lennert, A.; Guldi, D.M. Homoleptic and Heteroleptic Copper Complexes as Redox Couples in Dye-Sensitized Solar Cells. *ChemPhotoChem* **2019**, *3*, 636–644. [CrossRef]
79. Kuang, S.-M.; Cuttell, D.G.; McMillin, D.R.; Fanwick, P.E.; Walton, R.A. Synthesis and structural characterization of Cu(I) and Ni(II) complexes that contain the bis[2-(diphenylphosphino) phenyl]ether ligand novel emission properties for the Cu(I) species. *Inorg. Chem.* **2002**, *41*, 3313–3322. [CrossRef]
80. Xiao, P.; Dumur, F.; Zhang, J.; Gigmes, D.; Fouassier, J.-P.; Lalevée, J. Copper complexes: The effect of ligands on their photoinitiation efficiencies in radical polymerization reactions under visible light. *Polym. Chem.* **2014**, *5*, 6350–6357. [CrossRef]
81. Yang, Q.; Balverde, S.; Dumur, F.; Lalevée, J.; Poly, J. Synergetic effect of the epoxide functional groups in the photocatalyzed atom transfer radical copolymerization of glycidyl methacrylate. *Polym. Chem.* **2016**, *7*, 6084–6093. [CrossRef]

82. Al Mousawi, A.; Kermagoret, A.; Versace, D.-L.; Toufaily, J.; Hamieh, T.; Graff, B.; Dumur, F.; Gigmes, D.; Fouassier, J.-P.; Lalevée, J. Copper photoredox catalysts for polymerization upon near UV or visible light: Structure/reactivity/efficiency relationships and use in LED projector 3D printing resins. *Polym. Chem.* **2017**, *8*, 568–580. [CrossRef]
83. Chen, X.-L.; Yu, R.; Zhang, Q.-K.; Zhou, L.-J.; Wu, X.-Y.; Zhang, Q.; Lu, C.-Z. Rational design of strongly blue-emitting cuprous complexes with thermally activated delayed fluorescence and application in solution-processed OLEDs. *Chem. Mat.* **2013**, *25*, 3910–3920. [CrossRef]
84. Czerwieniec, R.; Leitl, M.J.; Homeier, H.H.H.; Yersin, H. Cu(I) complexes—Thermally activated delayed fluorescence. Photophysical approach and material design. *Coord. Chem. Rev.* **2016**, *325*, 2–28. [CrossRef]
85. Rehm, D.; Weller, A. Kinetics of fluorescence quenching by electron and H-Atom transfer. *Isr. J. Chem.* **1970**, *8*, 259–271. [CrossRef]
86. Mousawi, A.A.; Dietlin, C.; Graff, B.; Morlet-Savary, F.; Toufaily, J.; Hamieh, T.; Fouassier, J.-P.; Chachaj-Brekiesz, A.; Ortyl, J.; Lalevée, J. Meta-terphenyl derivative/iodonium salt/9H-carbazole-9-ethanol photoinitiating systems for free radical promoted cationic polymerization upon visible lights. *Macromol. Chem. Phys.* **2016**, *217*, 1955–1965. [CrossRef]
87. Fouassier, J.-P.; Lalevée, J. *Photoinitiators for Polymer Synthesis: Scope, Reactivity, and Efficiency*; John Wiley & Sons: Weinheim, Germany, 2013.
88. Fouassier, J.-P. *Photoinitiation, Photopolymerization, and Photocuring: Fundamentals and Applications*; Hanser: Munich, Germany, 1995.
89. Crivello, J.V.; Dietliker, K.; Bradley, G. *Photoinitiators for Free Radical Cationic & Anionic Photopolymerisation*; John Wiley & Sons: Chichester, UK, 1999.
90. Chen, L.; Yu, Q.; Wang, Y.; Li, H. BisGMA/TEGDMA dental composite containing high aspect-ratio hydroxyapatite nanofibers. *Dent. Mat.* **2011**, *27*, 1187–1195. [CrossRef]
91. Amirouche-Korichi, A.; Mouzali, M.; Watts, D.C. Shrinkage strain—Rates study of dental composites based on (BisGMA/TEGDMA) monomers. *Arab. J. Chem.* **2017**, *10*, S190–S195. [CrossRef]
92. Mello de Paiva Campos, L.; Cidreira Boaro, L.; Perez Ferreira, H.; Gomes dos Santos, L.K.; Ribeiro dos Santos, T.; Fernandes Parra, D. Evaluation of polymerization shrinkage in dental restorative experimental composites based: BisGMA/TEGDMA, filled with MMT. *J. Appl. Polym. Sci.* **2016**, *133*, 43543.
93. Sautrot-Ba, P.; Al Mousawi, A.; Lalevée, J.; Mazeran, P.-E.; Park, S.J.; Kang, I.-K.; Laurent-Brocq, M.; Langlois, V.; Versace, D.-L. Copper complex: A key role in the synthesis of biocidal polymer coatings. *Chem. Afr.* **2019**, *2*, 241–251.
94. Catilaz-Simonin, L.; Fouassier, J.-P. Investigation of a system capable of photoinitiating radical polymerizations in thick pigmented media. *J. Appl. Polym. Sci.* **2001**, *79*, 1911–1923. [CrossRef]
95. Grotzinger, C.; Burget, D.; Fouassier, J.-P. Polymerization activity in film and photochemical behaviour of a four components photoinitiating system. *Trends Photochem. Photobiol.* **2001**, *7*, 71–84.
96. Aguirre-Soto, A.; Lim, C.-H.; Hwang, A.T.; Musgrave, C.B.; Stansbury, J.W. Visible-light organic photocatalysis for latent radical-initiated polymerization via $2e^-/1H^+$ transfers: Initiation with parallels to photosynthesis. *J. Am. Chem. Soc.* **2014**, *136*, 7418–7427. [CrossRef] [PubMed]
97. Auerbach, S.S.; Bristol, D.W.; Peckham, J.C.; Travlos, G.S.; Hébert, C.D.; Chhabra, R.S. Toxicity and carcinogenicity studies of methylene blue trihydrate in F344N rats and B6C3F1 mice. *Food Chem. Toxicol.* **2010**, *48*, 169–177. [CrossRef] [PubMed]
98. Albert, M.; Lessin, M.S.; Gilchrist, B.F. Methylene blue: Dangerous dye for neonates. *J. Pediatr. Surg.* **2003**, *38*, 1244–1245. [CrossRef]
99. Ng, B.K.W.; Cameron, A.J.D. The role of methylene blue in serotonin syndrome: A systematic review. *Psychosomatics* **2010**, *51*, 194–200. [CrossRef]
100. Bynum, S.; Tullier, M.; Morejon-Garcia, C.; Guidry, J.; Runnoe, E.; Pojman, J.A. The effect of acrylate functionality on frontal polymerization velocity and temperature. *J. Polym. Sci. A Polym. Chem.* **2019**, *57*, 982–988. [CrossRef]
101. Riazi, H.; Shamsabadi, A.A.; Grady, M.C.; Rappe, A.M.; Soroush, M. Experimental and theoretical study of the self-initiation reaction of methyl acrylate in free-radical polymerization. *Ind. Eng. Chem. Res.* **2018**, *57*, 532–539. [CrossRef]

102. Mokbel, H.; Anderson, D.; Plenderleith, R.; Dietlin, C.; Morlet-Savary, F.; Dumur, F.; Gigmes, D.; Fouassier, J.P.; Lalevée, J. Copper photoredox catalyst "G1": A new high performance photoinitiator for near-UV and visible LEDs. *J. Polym. Chem.* **2017**, *8*, 5580–5592. [CrossRef]
103. Mokbel, H.; Anderson, D.; Plenderleith, R.; Dietlin, C.; Morlet-Savary, F.; Dumur, F.; Gigmes, D.; Fouassier, J.P.; Lalevée, J. Simultaneous initiation of radical and cationic polymerization reactions using the "G1" copper complex as photoredox catalyst: Applications of free radical/cationic hybrid photopolymerization in the composites and 3D printing fields. *Prog. Org. Coat.* **2019**, *132*, 50–61. [CrossRef]
104. Garra, P.; Dumur, F.; Mokbel, H.; Monnier, V.; Morlet-Savary, F.; Dietlin, C.; Gigmes, D.; Fouassier, J.P.; Lalevée, J. New synthetic route to a highly efficient photoredox catalyst by mechanosynthesis. *ACS Omega* **2018**, *3*, 10938–10944. [CrossRef]
105. Wang, G.-W. Mechanochemical organic synthesis. *Chem. Soc. Rev.* **2013**, *42*, 7668–7700. [CrossRef] [PubMed]
106. Šepelák, V.; Duüvel, A.; Wilkening, M.; Becker, K.-D.; Heitjans, P. Mechanochemical reactions and syntheses of oxides. *Chem. Soc. Rev.* **2013**, *42*, 7507–7520. [CrossRef] [PubMed]
107. Rightmire, N.R.; Hanusa, T.P. Advances in organometallic synthesis with mechanochemical methods. *Dalton Trans.* **2016**, *45*, 2352–2362. [CrossRef]
108. Friščić, T. Supramolecular concepts and new techniques in mechanochemistry: Cocrystals, cages, rotaxanes. open metal-organic frameworks. *Chem. Soc. Rev.* **2012**, *41*, 3493–3510. [CrossRef] [PubMed]
109. Delori, A.; Friščić, T.; Jones, W. The role of mechanochemistry and supramolecular design in the development of pharmaceutical materials. *CrystEngComm* **2012**, *14*, 2350–2362. [CrossRef]
110. Lazuen Garay, A.; Pichon, A.; James, S.L. Solvent-free synthesis of metal complexes. *Chem. Soc. Rev.* **2007**, *36*, 846–855. [CrossRef] [PubMed]
111. Baláž, P.; Achimovičová, M.; Baláž, M.; Billik, P.; Cherkezova-Zheleva, Z.; Criado, J.M.; Delogu, F.; Dutková, E.; Gaffet, E.; Gotor, F.J.; et al. Hallmarks of mechanochemistry: From nanoparticles to technology. *Chem. Soc. Rev.* **2013**, *42*, 7571–7637. [CrossRef]
112. Howard, J.L.; Cao, W.; Browne, D.L. Mechanochemistry as an emerging tool for molecular synthesis: What can it offer? *Chem. Sci.* **2018**, *9*, 3080–3094. [CrossRef]
113. Friščić, T.; Mottillo, C.; Titi, H.M. Mechanochemistry for Synthesis. *Angew. Chem. Int. Ed.* **2020**, *59*, 1018–1029. [CrossRef]
114. Do, J.-L.; Friščić, T. Mechanochemistry: A force of synthesis. *ACS Cent. Sci.* **2017**, *3*, 13–19. [CrossRef]
115. Štrukil, V.; Margetić, D.; Igrc, M.D.; Eckert-Maksić, M.; Friščić, T. Desymmetrisation of aromatic diamines and synthesis of nonsymmetrical thiourea derivatives by click-mechanochemistry. *Chem. Commun.* **2012**, *48*, 9705–9707. [CrossRef] [PubMed]
116. Shi, Y.X.; Xu, K.; Clegg, J.K.; Ganguly, R.; Hirao, H.; Friščić, T.; Garcia, F. The first synthesis of the sterically encumbered adamantoid phosphazane P4((NtBu)6: Enabled by mechanochemistry. *Angew. Chem. Int. Ed.* **2016**, *55*, 12736–12740. [CrossRef] [PubMed]
117. Katsenis, A.D.; Puškarić, A.; Štrukil, V.; Mottillo, C.; Julien, P.A.; Užarević, K.; Pham, M.-H.; Do, T.-O.; Kimber, S.A.J.; Lazić, P.; et al. In situ X-ray diffraction monitoring of a mechanochemical reaction reveals a unique topology metal-organic framework. *Nat. Commun.* **2015**, *6*, 6662. [CrossRef] [PubMed]
118. Wang, G.-W.; Komatsu, K.; Murata, Y.; Shiro, M. Synthesis and X ray structure of dumb-bell-shaped C120. *Nature* **1997**, *387*, 583–586. [CrossRef]
119. Tan, D.; Mottillo, C.; Katsenis, A.D.; Štrukil, V.; Friščić, T. Development of C-N coupling using mechanochemistry: Catalytic coupling of arylsulfonamides and carbodiimides. *Angew. Chem. Int. Ed.* **2014**, *53*, 9321–9324. [CrossRef]
120. Garra, P.; Dumur, F.; Morlet-Savary, F.; Dietlin, C.; Fouassier, J.-P.; Lalevée, J. A new highly efficient amine-free and peroxide-free redox system for free radical polymerization under air with possible light activation. *Macromolecules* **2016**, *49*, 6296–6309. [CrossRef]
121. Garra, P.; Dietlin, C.; Morlet-Savary, F.; Dumur, F.; Gigmes, D.; Fouassier, J.-P.; Lalevée, J. Redox two-component initiated free radical and cationic polymerizations: Concepts, reactions and application. *Prog. Polym. Sci.* **2019**, *94*, 33–56. [CrossRef]
122. Garra, P.; Dumur, F.; Nechab, M.; Morlet-Savary, F.; Dietlin, C.; Graff, B.; Doronina, E.P.; Sidorkin, V.F.; Gigmes, D.; Fouassier, J.-P.; et al. Peroxide-free and amine-free redox free radical polymerization: Metal acetylacetonates/stable carbonyl compounds for highly efficient synthesis of composites. *Macromolecules* **2018**, *51*, 6395–6404. [CrossRef]

123. Miller, G.A.; Gou, L.; Narayanan, V.; Scranton, A.B. Modeling of photobleaching for the photoinitiation of thick polymerization systems. *J. Polym. Sci. A Polym. Chem.* **2002**, *40*, 793–808. [CrossRef]
124. Cook, W.A.; Chen, F. Enhanced visible radiation photopolymerization of dimethacrylates with the three component thioxanthone (CPTXO)–amine–iodonium salt system. *Polym. Chem.* **2015**, *6*, 1325–1338. [CrossRef]
125. He, Y.; Zhou, W.; Wu, F.; Li, M.; Wang, E. Photoreaction and photopolymerization studies on squaraines dyes/iodonium salts combination. *J. Photochem. Photobiol. A Chem.* **2004**, *162*, 463–471. [CrossRef]
126. Bonardi, A.-H.; Bonardi, F.; Dumur, F.; Gigmes, D.; Lalevée, J. Fillers as heaters for photothermal polymerization upon NIR light. *Macromol. Rapid. Commun.* **2019**, *40*, 1900495. [CrossRef] [PubMed]
127. Bonardi, A.-H.; Bonardi, F.; Noirbent, G.; Dumur, F.; Dietlin, C.; Gigmes, D.; Fouassier, J.-P.; Lalevée, J. Different NIR dye scaffolds for polymerization reactions under NIR light. *Polym. Chem.* **2019**, *10*, 6505–6514. [CrossRef]
128. Mokbel, H.; Dumur, F.; Lalevée, J. On demand NIR activated photopolyaddition reactions. *Polym. Chem.* **2020**, *11*, 4250–4259. [CrossRef]
129. Kim, J.U.; Park, I.S.; Chan, C.Y.; Tanaka, M.; Tsuchiya, Y.; Nakanotani, H.; Adachi, C. Nanosecond-time-scale delayed fluorescence molecule for deep-blue OLEDs with small efficiency rolloff. *Nat. Commun.* **2020**, *11*, 1765. [CrossRef]
130. Yang, Z.; Mao, Z.; Xie, Z.; Zhang, Y.; Liu, S.; Zhao, J.; Xu, J.; Chi, Z.; Aldred, M.P. Recent advances in organic thermally activated delayed fluorescence materials. *Chem. Soc. Rev.* **2017**, *46*, 915–1016. [CrossRef]
131. Liang, X.; Tu, Z.-L.; Zheng, Y.-X. Thermally activated delayed fluorescence materials: Towards realization of high efficiency through strategic small molecular design. *Chem. Eur. J.* **2019**, *25*, 5623–5642. [CrossRef]
132. Congrave, D.G.; Drummond, B.H.; Conaghan, P.J.; Francis, H.; Jones, S.T.E.; Grey, C.P.; Greenham, N.C.; Credgington, D.; Bronstein, H. A Simple Molecular Design Strategy for Delayed Fluorescence toward 1000 nm. *J. Am. Chem. Soc.* **2019**, *141*, 18390–18394. [CrossRef]
133. Adachi, C. Third-generation organic electroluminescence materials. *Jap. J. Appl. Phys.* **2014**, *53*, 060101. [CrossRef]
134. Parker, C.A.; Hatchard, C.G. Triplet-singlet emission in fluid solutions. Phosphorescence of eosin. *Trans. Faraday Soc.* **1961**, *57*, 1894–1904. [CrossRef]
135. Nakanotani, H.; Masui, K.; Nishide, J.; Shibata, T.; Adachi, C. Promising operational stability of high-efficiency organic light-emitting diodes based on thermally activated delayed fluorescence. *Sci. Rep.* **2013**, *3*, 2127. [CrossRef] [PubMed]
136. Al Mousawi, A.; Magaldi Lara, D.; Noirbent, G.; Dumur, F.; Toufaily, J.; Hamieh, T.; Bui, T.-T.; Goubard, F.; Graff, B.; Gigmes, D.; et al. Carbazole derivatives with thermally activated delayed fluorescence property as photoinitiators/photoredox catalysts for LED 3D printing technology. *Macromolecules* **2017**, *50*, 4913–4926. [CrossRef]
137. Bonardi, A.-H.; Dumur, F.; Noirbent, G.; Lalevée, J.; Gigmes, D. Organometallic vs. organic photoredox catalysts for photocuring reactions in the visible region. *Beilstein J. Org. Chem.* **2018**, *14*, 3025–3046. [CrossRef] [PubMed]
138. Bouzrati-Zerelli, M.; Noirbent, G.; Goubard, G.; Bui, T.-T.; Villotte, S.; Dietlin, C.; Morlet-Savary, F.; Gigmes, D.; Fouassier, J.-P.; Dumur, F.; et al. A novel class of photoinitiators with a thermally activated delayed fluorescence (TADF) property. *New J. Chem.* **2018**, *42*, 8261–8270. [CrossRef]
139. Linfoot, C.-L.; Leitl, M.-J.; Richardson, P.; Rausch, A.-F.; Chepelin, O.; White, F.-J.; Yersin, H.; Robertson, N. Thermally activated delayed fluorescence (TADF) and enhancing photoluminescence quantum yields of $[CuI(diimine)(diphosphine)]^+$ complexes-photophysical, structural, and computational studies. *Inorg. Chem.* **2014**, *53*, 10854–10861. [CrossRef] [PubMed]